




A novel stem cell type at the basal side of the subventricular zone maintains adult neurogenesis

Katja Baur¹ , Yomn Abdullah^{1,‡}, Claudia Mandl¹, Gabriele Hölzl-Wenig¹, Yan Shi^{1,§}, Udo Edelkraut^{1,¶}, Priti Khatri^{1,#}, Anna M Hagenston¹ , Martin Imler², Johannes Beckers^{2,3,4} & Francesca Ciccolini^{1,*} 

Abstract

According to the current consensus, murine neural stem cells (NSCs) apically contacting the lateral ventricle generate differentiated progenitors by rare asymmetric divisions or by relocating to the basal side of the ventricular–subventricular zone (V–SVZ). Both processes will ultimately lead to the generation of adult-born olfactory bulb (OB) interneurons. In contrast to this view, we here find that adult-born OB interneurons largely derive from an additional NSC-type resident in the basal V–SVZ. Despite being both capable of self-renewal and long-term quiescence, apical and basal NSCs differ in Nestin expression, primary cilia extension and frequency of cell division. The expression of Notch-related genes also differs between the two NSC groups, and Notch activation is greatest in apical NSCs. Apical downregulation of Notch-effector *Hes1* decreases Notch activation while increasing proliferation across the niche and neurogenesis from apical NSCs. Underscoring their different roles in neurogenesis, lactation-dependent increase in neurogenesis is paralleled by extra activation of basal but not apical NSCs. Thus, basal NSCs support OB neurogenesis, whereas apical NSCs impart Notch-mediated lateral inhibition across the V–SVZ.

Keywords neural stem cells; neurogenesis; notch signalling; olfactory bulb; subventricular zone

Subject Categories Neuroscience; Stem Cells & Regenerative Medicine

DOI 10.15252/embr.202154078 | Received 1 October 2021 | Revised 20 June 2022 | Accepted 4 July 2022

EMBO Reports (2022) e54078

Introduction

The adult mammalian brain, despite being generally unable to repair and regenerate, encompasses self-renewing and multipotent neural stem cells (NSCs) (Gage, 2002; Oberner & Alvarez-

Buylla, 2019). In mice, NSCs were initially retrospectively identified by means of clonal assays, demonstrating that epidermal growth factor (EGF) elicits the proliferation of rare self-renewing and multipotent adult brain cells (Reynolds & Weiss, 1992). Thereafter, it was shown that NSCs residing in the subgranular zone (SGZ) of the hippocampus and the ventricular–subventricular zone (V–SVZ) lining the lateral ventricles sustain neurogenesis throughout adulthood (Ming & Song, 2011). The latter represents the largest neurogenic niche in the adult murine brain, where adult-born neuroblasts migrate along the rostral migratory stream to the olfactory bulb (OB) where they differentiate into GABAergic and, to a lesser extent, glutamatergic interneurons (Lois *et al.*, 1996; Merkle *et al.*, 2007; Brill *et al.*, 2009). Underscoring its functional relevance, adult OB neurogenesis contributes to odour recognition (Feierstein, 2012) and it is modulated by behaviour engaging the olfactory function like during mating and parenting (Shingo *et al.*, 2003; Furuta & Bridges, 2005).

Most cells in the adult murine brain originate from radial glia progenitors (Malatesta *et al.*, 2003; Anthony *et al.*, 2004). Radial glia cells displaying apical–basal polarity are first generated at the onset of neurogenesis between embryonic days (E) 10 and 12 (Kriegstein & Gotz, 2003). They are characterized by an apically located centrosome as well as Nestin (Hockfield & McKay, 1985) and Prominin-1 (Weigmann *et al.*, 1997) expression. The astroglial marker glial fibrillary acidic protein (GFAP) is first expressed in this population after birth when many radial glia cells transform into astrocytes (Misson *et al.*, 1991; Kalman & Pritz, 2001; Alves *et al.*, 2002).

Radial glia cells also give rise to adult apical radial glia-like NSCs (Merkle *et al.*, 2007; Ortiz-Alvarez *et al.*, 2019), which maintain apical–basal polarity, cilia extension and can be labelled with Nestin and Prominin-1. After birth, these NSCs additionally express GFAP and are often referred to as type B1 astrocytes (Mirzadeh *et al.*, 2008; Shen *et al.*, 2008; Tavazoie *et al.*, 2008). In the adult V–SVZ, proliferating NSCs and especially more differentiated intermediate progenitors, including transit-amplifying progenitors (TAPs) and pre-neuroblasts, display high EGF receptor (EGFR)

¹ Department of Neurobiology, Interdisciplinary Center for Neurosciences, Heidelberg University, Heidelberg, Germany

² Helmholtz Zentrum München GmbH, Institute of Experimental Genetics, Neuherberg, Germany

³ Technische Universität München, Chair of Experimental Genetics, Weihenstephan, Germany

⁴ Deutsches Zentrum für Diabetesforschung e.V. (DZD), Neuherberg, Germany

*Corresponding author. Tel: +49-6221-548696; Fax: +49-6221-546700; E-mail: ciccolini@nbio.uni-heidelberg.de

[‡]Present address: Division of Systems Biology of Signal Transduction, German Cancer Research Center (DKFZ), Heidelberg, Germany

[§]Present address: Department of Human Genetics, Radboud University Medical Center, Nijmegen, The Netherlands

[¶]Present address: Molecular Health GmbH, Heidelberg, Germany

[#]Present address: ICGC lab, Advanced Centre for Treatment, Research and Education in Cancer, Tata Memorial Centre, Navi Mumbai, India

levels which are downregulated during neuronal differentiation (Doetsch *et al*, 1999; Cesetti *et al*, 2009; Carrillo-Garcia *et al*, 2010; Codega *et al*, 2014; Khatri *et al*, 2014).

Genetic tagging has shown that cells displaying GFAP promoter activity contribute to neurogenesis in the olfactory bulb (OB) (Doetsch *et al*, 1999; Garcia *et al*, 2004; Beckervordersandforth *et al*, 2010; Weber *et al*, 2011). However, it is unclear whether these tagged cells represent apical radial glia-like NSCs (Joppe *et al*, 2020). Notably, so-called type B2 astrocytes expressing GFAP are also present at the basal side of the V-SVZ. Although they can proliferate (Doetsch *et al*, 1997), and some undergo quiescence (Obernier *et al*, 2018), it is unknown whether they are neurogenic and have been generally included in the population of niche astrocytes (Beckervordersandforth *et al*, 2010).

Moreover, during embryonic development, apical radial glia can give rise to basal radial glia that lack apical attachment, undergo mitosis at the basal side of the niche and are critical for the numeric expansion of neurons in gyrencephalic brains (Florio & Huttner, 2014; Penisson *et al*, 2019). The generation of basal progenitors from apical NSCs has also been observed in the V-SVZ of neonatal (Alves *et al*, 2002; Tramontin *et al*, 2003) and in older mice (Obernier *et al*, 2018). However, in both cases, rather than with asymmetric self-renewing division of apical NSCs, the generation of these basal progenitors is associated with apical NSC consumption.

In contrast to this model, we here show the presence of a NSC lacking apical attachment which is capable of undergoing long-term quiescence, activation and self-renewal at the basal side of the postnatal V-SVZ. From birth onwards, these basal NSCs form the largest NSC pool in the postnatal V-SVZ and the main source of adult-born OB neuroblasts. Moreover, the temporary increase in proliferation, which occurs in the V-SVZ following lactation (Shingo *et al*, 2003), is sustained by the activation of basal NSCs. Our data show that apical NSCs contribute to niche homeostasis by regulating levels of Notch-mediated lateral inhibition across the V-SVZ.

Results

The majority of hGFAP-tagged progenitors display no apical membrane and no Prominin-1 immunoreactivity

Adult NSCs were firstly examined in 8-weeks-old (8W) hGFAP;H2B-GFP mice, in which the tetracycline-responsive transactivator (tTA)

expressed from a human GFAP promoter controls the transcription of histone 2B fused to the green fluorescent protein (H2B-GFP) in a Tet-off fashion (Luque-Molina *et al*, 2017). Supporting the specificity of the reporter system, GFP-H2B expression was only observed in cells with tTA nuclear immunoreactivity, and the latter was no longer visible upon administration of doxycycline (Appendix Fig S1A). To be able to identify cells contacting the lateral ventricle, apical membranes were additionally labelled by applying DiI on the apical side of the intact V-SVZ (Fig 1A–C) and, after tissue dissection and dissociation, by Prominin-1 immunostaining (Fig 1D–F), as previously reported (Khatri *et al*, 2014). The H2B-GFP-expressing (G^+) NSCs were a small minority of the total viable cells (Fig 1A). Nevertheless, compared to the remaining G^- cells, they were significantly enriched in DiI^+ apical cells (Fig 1B), representing $23.54\% \pm 2.62$ of the total DiI^+ cells (Fig 1C). Similarly, the incidence of Prominin-1-immunopositive (P^+) cells was higher in the G^+ population than in the remaining G^- cells (Fig 1D and E), and the majority of G^+P^+ cells were DiI^+ (Fig 1F), which is consistent with Prominin-1 being prominently expressed in apical V-SVZ cells. However, the majority of H2B-GFP-tagged cells neither expressed Prominin-1 (Fig 1E) nor displayed DiI labelling (Fig 1B), indicating that they are basal progenitors lacking an apical attachment. Our observation that most tagged cells lack Prominin-1 immunostaining is consistent with previous findings (Beckervordersandforth *et al*, 2010). However, this previous study concluded that, among the hGFAP-GFP-tagged cells in the V-SVZ, only double-positive Prominin-1/GFP+ cells were NSCs, whereas the Prominin-1/GFP- counterpart represented niche astrocytes. This conclusion was supported by the differences in the gene expression profile between Prominin-1/GFP+ NSCs and GFP+ astrocytes isolated from the diencephalon. However, no direct comparison was performed between Prominin-1/GFP+ cells and GFP+ diencephalic astrocytes. Therefore, we mined the previously published data to perform this analysis. A principal component analysis (PCA) showed that independent of Prominin-1 expression, GFP+ cells in the V-SVZ are similarly divergent from diencephalic astrocytes (Appendix Fig S1B). Moreover, analysis of differentially regulated genes between the two GFP+ populations in the V-SVZ highlighted a significant regulation of genes associated with chromosome replication and mitosis in Prominin-1/GFP+ (Appendix Table S1 and Dataset EV1). The signalling pathways activated in Prominin-1/GFP+ cells also included those involving the epidermal growth factor (EGF) and the antiangiogenic pigment epithelium-derived factor (PEDF), previously shown to act as a niche-derived growth factor promoting NSC self-renewal

Figure 1. Most hGFAP-tagged cells display neither an apical membrane nor Prominin-1 expression.

- A Representative FACS plot illustrating the distribution of dissociated V-SVZ cells according to their H2B-GFP (GFP) and DiI fluorescence (middle panel) and a control lacking DiI staining (left panel). Quantitative analysis in the right panel shows the total number of V-SVZ cells expressing (G^+) or not expressing H2B-GFP (G^-).
- B, C Quantitative analysis of the percentage of DiI-labelled (DiI^+) apical cells within G^- and G^+ populations (B) and of the percentage of G^- and G^+ among total apical (DiI^+) and basal (DiI^-) V-SVZ cells (C).
- D Representative FACS plot of G^- cells (left panels) and G^+ cells (right panels) illustrating their distribution according to Prominin-1 and DiI fluorescence after DiI staining of the apical membrane without (top) and with Prominin-1 staining (bottom).
- E Quantification of the percentage of Prominin-1-immunopositive cells in G^- and G^+ populations.
- F Quantitative analysis of the percentage of DiI^+ apical cells in each G^- and G^+ population sorted additionally on the basis of Prominin-1 (P) expression.

Data information: Data are represented as mean \pm SEM. $N = 29$ biological replicates. *Indicates significance between apical (DiI^+) and basal (DiI^-) cells within the same cell population and # indicates significance between G^- and G^+ in (B) and between G^-P^+ and G^-P^- or G^+P^+ and G^+P^- in (F). ** $P < 0.01$, ***/#### $P < 0.001$, determined by two-tailed unpaired Student's t -test (A, E) or two-way ANOVA with Sidak's multiple comparisons test (B, F).

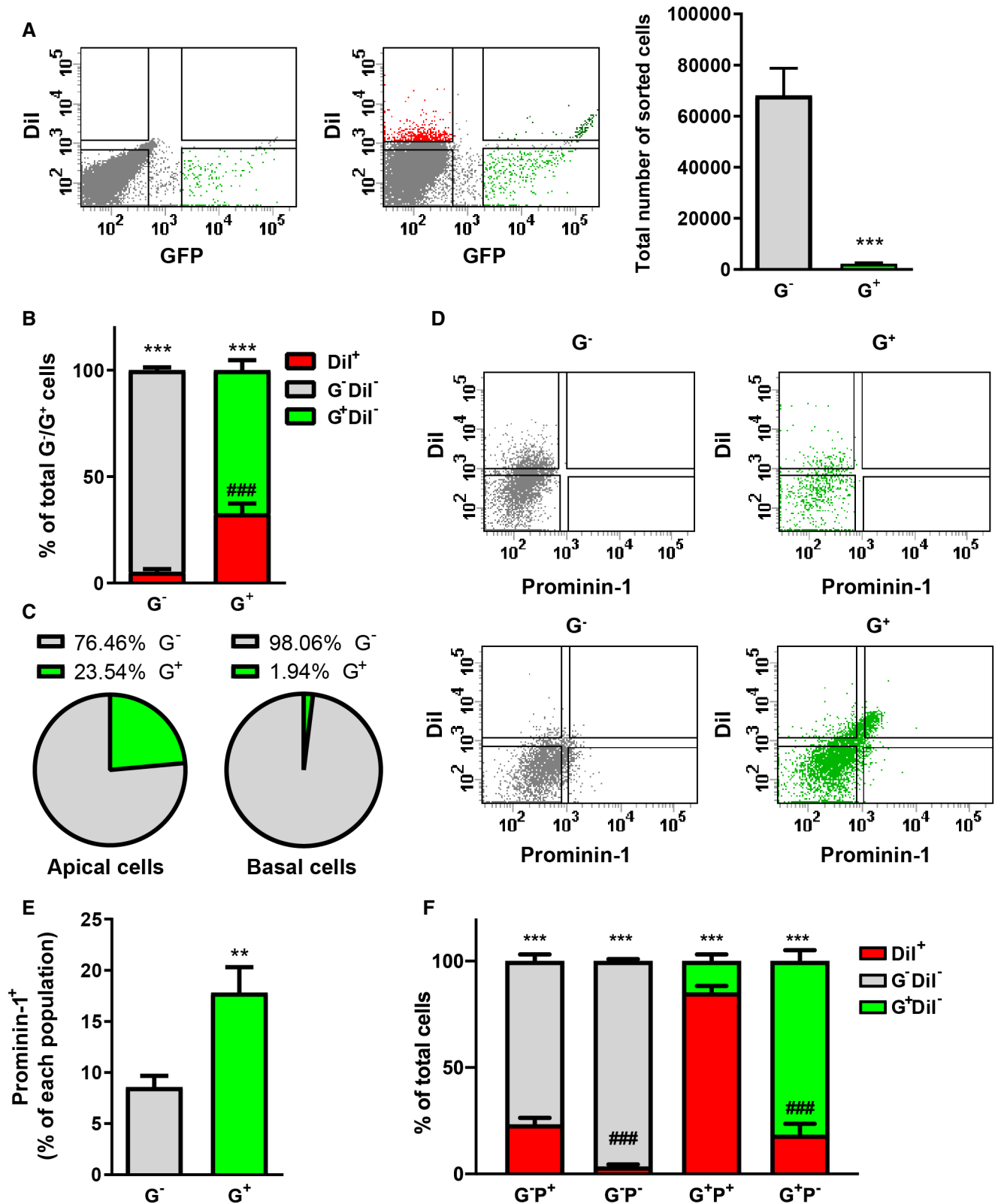


Figure 1.

(Ramirez-Castillejo *et al*, 2006). Thus, basal Prominin⁻/hGFAP-tagged cells in the V-SVZ display a transcriptional profile compatible with stemness.

Both apical and basal hGFAP-tagged progenitors display hallmarks of NSCs

To directly investigate the possibility that basal progenitors include NSCs, we next analysed the characteristics of G⁺ cells in slices of the V-SVZ obtained from mice that had been administered doxycycline for the previous 30 days and from untreated animals. Labelled nuclei were considered to belong to apical progenitors if they were localized at a maximal distance from the ventricle of 10 μm along the apical–basal axis, as determined based on the analysis of the position of the nuclei of apical cells tagged by intraventricular injection of adeno-associated virus (AAV) carrying a green fluorescent protein (GFP) reporter gene (Appendix Fig S1C and D; Luque-Molina *et al* (2019)). We firstly examined the expression of NSC markers like GFAP, the sex-determining region Y (SRY)-box transcription factor 9 (SOX9) (Scott *et al*, 2010) (Appendix Fig S2), and Nestin (Fig 2A and B), which is observed especially in actively cycling NSCs (Codega *et al*, 2014). Double-positive Nestin⁺/G⁺ cells were apical and were significantly reduced upon doxycycline administration (Fig 2A and B). A similar trend was observed for GFAP and SOX9 expression, but it was not significant as basal cells expressed more GFAP and SOX9 than Nestin (Appendix Fig S2A–C and Fig 2A and B). Finally, both groups of G⁺ cells expressed similar transcript levels of the Leucine-rich repeats and immunoglobulin-like domains 1 (Lrig1) gene (Appendix Fig S2D), which is also a marker for the prospective identification of NSCs in the V-SVZ (Nam & Capecchi, 2020). Instead, at either side of the niche, very few tagged cells expressed the differentiation marker doublecortin (DCX) (apical: 0.8 ± 0.4; basal 2.8 ± 1.4; N = 3) and administration of doxycycline led to a trend increase which was not significant (apical: 3.1 ± 1.3; basal 5.5 ± 0.9; N = 3).

A subset of quiescent NSCs in the adult V-SVZ also displays primary cilia (Khatri *et al*, 2014), and cilia signalling is upregulated in NSCs of the V-SVZ closely linked to cell cycle progression and signal transduction (Goto *et al*, 2013). Therefore, we next used adenylate cyclase 3 (AC3) as a primary cilia marker (Bishop *et al*, 2007; Monaco *et al*, 2019) in combination with Nestin and H2B-GFP to investigate the presence of primary cilia in apical and basal progenitors (Fig 2C–E). Ciliated progenitors represented a small subset of G⁺-tagged progenitors in the V-SVZ and they were more abundant at

the apical side of the niche (Fig 2D). A similar association between apical NSCs and primary cilia was observed also in WT mice, where ciliated cells were enriched within DiI⁺ labelled apical cells (Appendix Fig S2E and F). However, on either side of the niche, G⁺ and/or Nestin⁺ progenitors still represented a consistent proportion of the ciliated cells especially on the basal side (Fig 2E).

We next investigated whether basal G⁺ progenitors undergo quiescence and self-renewal, which are defining functional properties of NSCs. We first measured label retention and Ki67 expression in each progenitor population. To examine label-retaining cells, we took advantage of the fact that, upon transcriptional downregulation, the fluorescent nuclear H2B-GFP signal disappears after five cell divisions (Waghmare *et al*, 2008) and measured the number of total apical or basal G⁺ cells in mice that had been administered doxycycline for 30 days and in untreated controls. The treatment led to a small reduction in the number of total G⁺ cells and a parallel increase in the number of total G⁻ cells, which was significant only within the subset of basal progenitors (Fig 3A and B) and to an overall decrease in levels of H2B-GFP expression in both cell populations (Appendix Fig S3A and B), suggesting that also apical cells G⁺ undergo fewer cell divisions during the treatment than basal G⁺ cells. Supporting the concept that cell division critically affects reporter expression levels, apical- and basal-tagged progenitors contained a similar percentage of mitotic cells, especially in the subset of cells expressing high levels of reporter (Appendix Fig S3C–E). Apical and basal G⁺ progenitors also contained a similar percentage of Ki67⁺ cycling cells, and doxycycline treatment led again to a significant reduction in the number of cycling cells only in basal G⁺ progenitors (Fig 3C), which is to be expected if basal Ki67⁺ cycling cells undergo more rounds of cell divisions, thereby losing the nuclear labelling. Taken together, these data indicate that both populations, in addition to label-retaining cells, also contain cells that within a month undergo a few cell divisions, a process leading to a loss of nuclear labelling in a subset of basal G⁺ progenitors. It is known that quiescent adult NSCs include slow-cycling radial glia progenitors which enter quiescence at mid-development (Fuentelba *et al*, 2015; Furutachi *et al*, 2015; Hu *et al*, 2017; Yuzwa *et al*, 2017). We, therefore, labelled proliferating cells with a single IdU injection at embryonic day (E)14. Analysis of the V-SVZ of the injected hGFAP;H2B-GFP mice performed 8 weeks after birth revealed label retention in the nuclei of apical and basal G⁺ progenitors, showing that both populations also include long-term quiescent cells (Fig 3D). Moreover, consistent with previous observations, the number of double-labelled cells was reduced if mice were injected at E18 (Fuentelba

Figure 2. Basal NSCs in the adult V-SVZ do not express Nestin and do not extend primary cilia.

- A Representative confocal photomicrographs showing coronal slices from 8 W hGFAP-tTA;H2B-GFP mice with and without doxycycline treatment, upon immunofluorescent staining with the stem cell marker Nestin (red). DAPI was used for nuclear counterstain. Cross indicates slice directions: M = medial, D = dorsal, V = ventral, L = lateral. Scale bar = 20 μm.
- B Quantification of Nestin expression in apical and basal cells in doxycycline-treated and untreated animals. N = 3 (– Doxy), N = 4 (+ Doxy).
- C Same as (A), with the addition of the primary cilia marker AC3 (yellow). Arrows indicate Nestin-positive (white) and GFP-positive (green) cells with primary cilium. Scale bar = 10 μm.
- D Quantification of ciliated GFP⁺ NSCs in apical and basal cell layer as percentage of total apical/basal GFP⁺ cells. N = 7.
- E Quantification of primary cilia on cells in the apical or basal cell layer according to stem cell marker; N = 7.

Data information: N refers to number of biological replicates; for each biological replicate, at least three technical replicates were performed. Data are represented as mean ± SEM. * and # indicate significance: between apical and basal (*) and between doxycycline treatments (#); *[#]P < 0.05, **P < 0.01, by one-way ANOVA with Tukey's multiple comparisons test (B) or two-tailed unpaired Student's t-test (D).

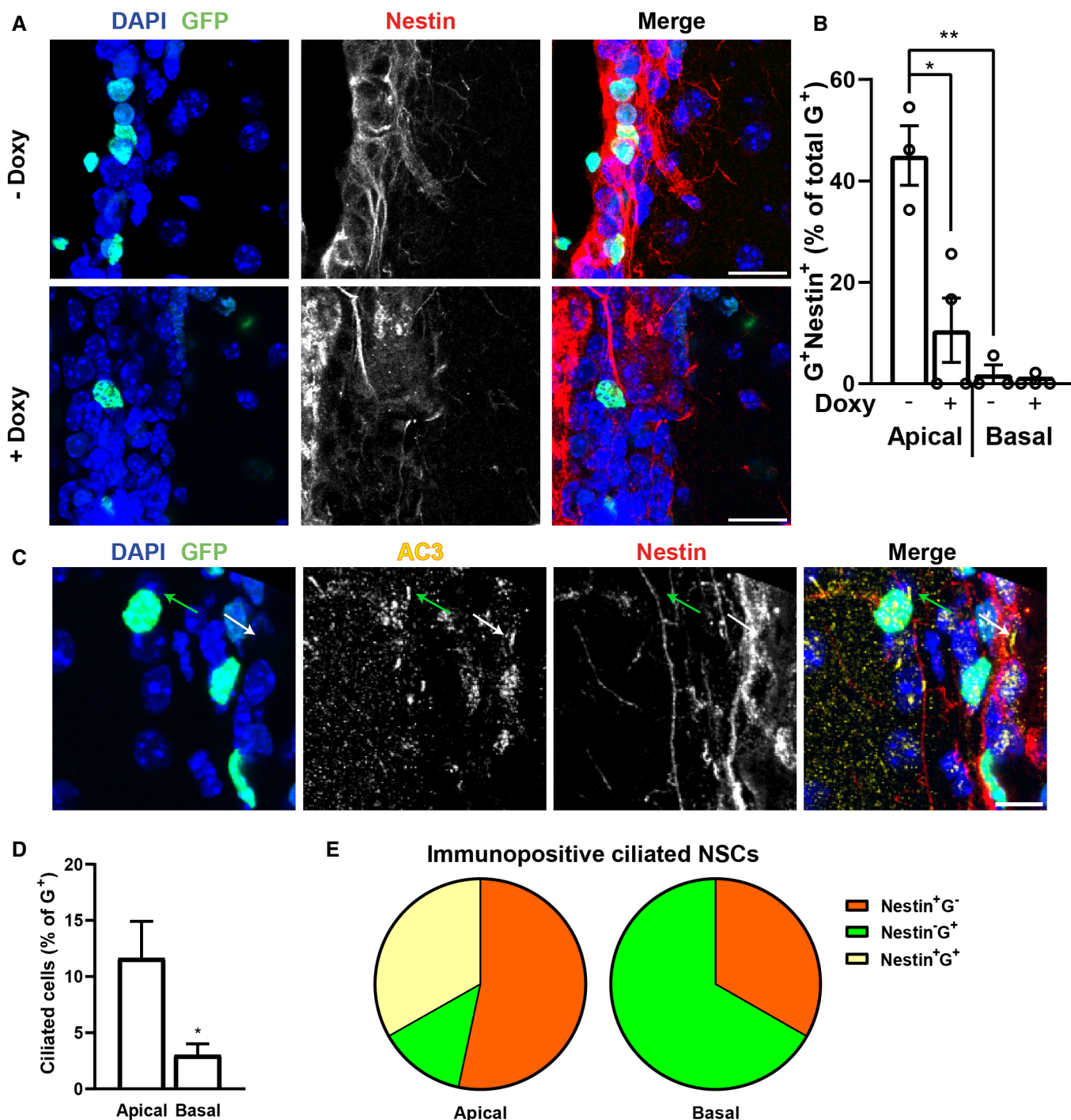


Figure 2.

et al, 2015; Furutachi et al, 2015) (Fig 3D). Thus, apical and basal G^+ progenitors both contain progenitors undergoing long- and short-term quiescence.

To analyse the self-renewal *in vivo*, we reasoned that in control untreated mice, self-renewing divisions would maintain high levels of reporter expression in G^+ cells, whereas non-renewing cell division, comparable to doxycycline administration, would cause a gradual dilution in fluorescence levels at each cell division.

Therefore, to measure the self-renewal rate, we firstly compared the percentage of G^+ cells expressing high (G^h) or intermediate (G^i) fluorescence levels by flow cytometry as described before (Luque-Molina et al, 2017), see also “Methods” section, in sorted apical P^+G^+ and basal P^-G^+ progenitors (Fig 3E), and by immunohistochemistry in apical and basal G^+ progenitors in brain slices (Fig 3F). Both approaches showed that compared to doxycycline-treated animals, control untreated mice displayed a consistent increase in the

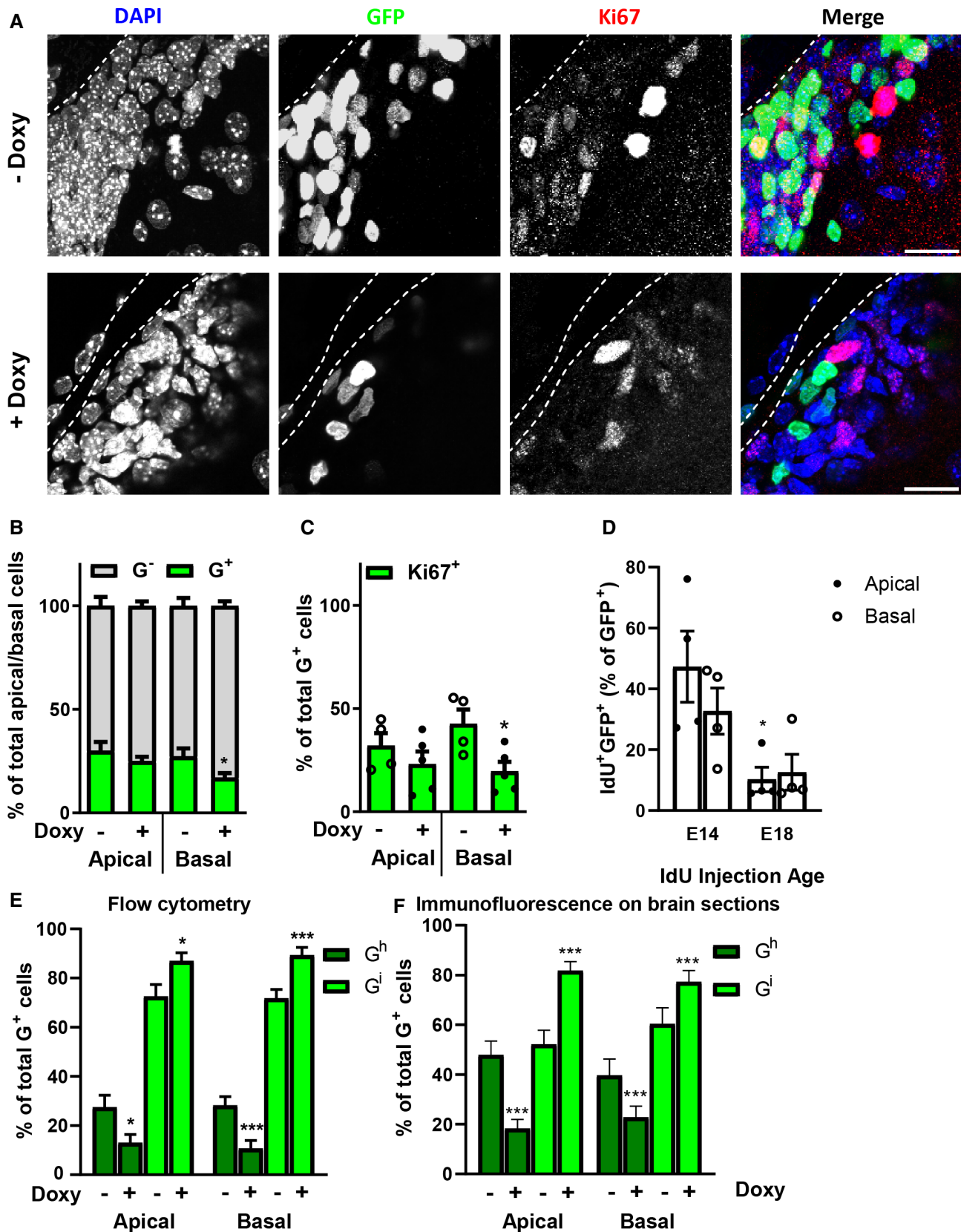


Figure 3.

Figure 3. Apical and basal NSCs display stemness.

- A Representative confocal photomicrographs of coronal sections of the V-SVZ of 8 W hGFAP-H2BGFP mice, which had been administered doxycycline (Doxy) as indicated. Nuclear GFP expression and Ki67 immunoreactivity are shown in green and red respectively. DAPI counterstaining of the nuclei is blue. Scale bar indicates 20 μm .
- B, C Quantitative analyses of the number of apical and basal cells expressing GFP (G^+) or not (G^-); $N = 8$ (B), and Ki67 immunoreactivity in these populations; $N \geq 4$ (C).
- D Quantitative analysis of the number of label-retaining apical and basal G^+ cells in mice injected with IdU at embryonic day E14 or E18 and analysed 8 W after birth. $N = 4$.
- E, F Quantification of the percentage of apical and basal G^+ cells expressing intermediate (G^i) or high (G^h) GFP levels with or without doxycycline (Doxy) treatment upon FACS analysis; $N \geq 21$ (E) and in brain slices; $N = 7$ (– Doxy), 9 (+ Doxy; F).

Data information: N refers to number of biological replicates; for each biological replicate (except E), at least three technical replicates were performed. Bars represent mean \pm SEM. *Indicates significance between doxycycline-treated and nontreated specimens with apical or basal cell populations. * $P < 0.05$, *** $P < 0.001$, determined by two-way ANOVA with Sidak's multiple comparisons test.

percentage of G^h cells within both apical and basal progenitors, indicating that both cell groups undergo self-renewal *in vivo*. Indeed, in the presence of doxycycline, the percentage of G^i cells expressing the NSC markers GFAP and SOX9 remained the same in apical and basal G^+ progenitors, as expected if these cells underwent self-renewing cell divisions (Appendix Fig S3F).

Neurosphere formation is a hallmark property of proliferating adult NSCs (Codega *et al.*, 2014; Khatri *et al.*, 2014). Therefore, we next tested the ability of apical and basal G^+ precursors to form clonal neurospheres (Appendix Fig S3G and H). For this analysis, cells were additionally sorted between those expressing high (E^h) and low (E^l) EGFR levels, as the first are enriched in clone-forming cells compared to the latter (Ciccolini *et al.*, 2005). When isolated from control mice, both basal $G^+P^-E^h$ and $G^+P^-E^l$ progenitors generated clones, albeit with different frequencies. Instead, consistent with previous observations in WT progenitors (Khatri *et al.*, 2014), apical $G^+P^+E^h$ but not $G^+P^+E^l$ progenitors underwent clone formation, indicating that the latter maintain a slow rate of cell division also *in vitro*. Notably, when G^+ cells were isolated from doxycycline-treated mice, clone formation was drastically reduced and almost exclusively observed in the group of $G^+P^-E^h$ cells, supporting the notion that quiescent NSCs are not capable of forming clones and that most activated NSCs display high levels of EGFR. Clones grew extensively *in vitro* and could be frozen and thawed for further propagation, in line with the fact that NSCs are endowed with extensive proliferation. Independent of niche location, G^+E^h cells displayed higher Mash-1 expression levels than the G^+E^l counterpart (Appendix Fig S3I), confirming that they represent activated NSCs. Taken together, these data show that basal G^+ precursors display characteristics of adult NSCs, including the ability to undergo quiescence, self-renewal and clone formation when they are in an active state. Therefore, they will be hereafter referred to as basal NSCs.

Basal NSCs represent the predominant NSC population throughout postnatal life

It has been recently shown that in the adult V-SVZ, apical NSCs increasingly give rise to basal progenitors which are label-retaining cells and display levels of GFAP expression similar to basal NSCs (Obernier *et al.*, 2018). Therefore, we next investigated if basal NSCs are generated from apical NSCs during adulthood or if they are already present early on in the neonatal brain. We first analysed the presence of apical and basal NSCs in slices of the V-SVZ of 1-W-old hGFAP;H2B-GFP mice (Appendix Fig S4). Quantitative analysis showed not only that apical and basal G^+ NSCs are already present

at this early age but also that the two groups show differences with respect to Nestin expression (Appendix Fig S4A and B), ciliation (Appendix Fig S4A–C) and prevalence of G^+ cells within ciliated progenitors (Appendix Fig S4D). Although these differences were similar in trend to those observed in their adult counterparts, they varied in absolute values. Independent of the niche location, neonatal cells displayed a greater proportion of G^+ cells co-expressing Nestin and extending a primary cilium than the relative group in adult mice. Taken together, these data show that cells with defining characteristics of basal and apical NSCs are already present in the V-SVZ of neonatal mice.

We next investigated age-related changes in the number of apical and basal NSCs and their propensity to undergo activation. To this end, we quantified the number of apical G^+P^+ and basal G^+P^- progenitors (Fig 4A left panel) and the proportion of each population expressing high EGFR levels at the cell surface (E^h ; Fig 4A right panel) at various postnatal ages. Consistent with previous observations in WT mice (Carrillo-Garcia *et al.*, 2010), the number of basal and apical NSCs decreased with age (Fig 4A left panel). However, for both apical and basal NSCs, the sharpest and only significant drop in NSC numbers occurred between 1 and 2 weeks after birth, similar to what was recently reported for hippocampal NSCs (Harris *et al.*, 2021). In contrast, a significant decrease in the proportion of activated NSCs was observed first in 8W animals, affecting basal NSCs only, and thereafter in 25W mice for both apical and basal NSCs (Fig 4A). We next determined the effect of age on the potential of proliferation and self-renewal of apical and basal NSCs with clonal assays (Fig 4B–D). For this analysis, apical and basal NSCs were sorted from the V-SVZ of 8W and 25W to 30W animals by flow cytometry based also on Dil labelling of the apical membrane as well as EGFR and Prominin-1 expression. Consistent with our previous analysis, age led to a decrease in the number of activated $G^+P^-E^h$ cells within the basal (D^-) but not apical (D^+) pool of NSCs (Fig 4B). At both ages, all types of NSCs generated clones and, in line with our findings *in vivo*, they were also able to undergo self-renewal *in vitro*, determined by the number of green cells per clone (Fig 4C and D). However, unlike the remaining populations, apical $G^+P^+E^h$ NSCs underwent very limited self-renewal (Fig 4C) and generated only small clones when isolated from older mice (Fig 4D left panel). A similar trend towards a decrease in the ability to generate large clones was also observed for basal $G^+P^+E^h$ NSCs. Moreover, in basal $G^+P^-E^h$ NSCs, age led to a significant increase in the proportion of cells capable of generating large clones (Fig 4D right panel). Taken together, these data show that basal NSCs represent the major NSC population in the postnatal V-SVZ throughout

adulthood. Independent of their location in the V-SVZ, between 2 and 25 weeks after birth, the number of NSCs remains essentially constant. However, age affects the ability of both NSC groups to express high levels of EGFR and the proliferation potential of apical NSCs.

Basal NSCs derive from apical NSCs and are the main contributors to neurogenesis

Several studies have previously shown that the GFAP-expressing NSCs in the V-SVZ give rise to OB interneurons. For example, we

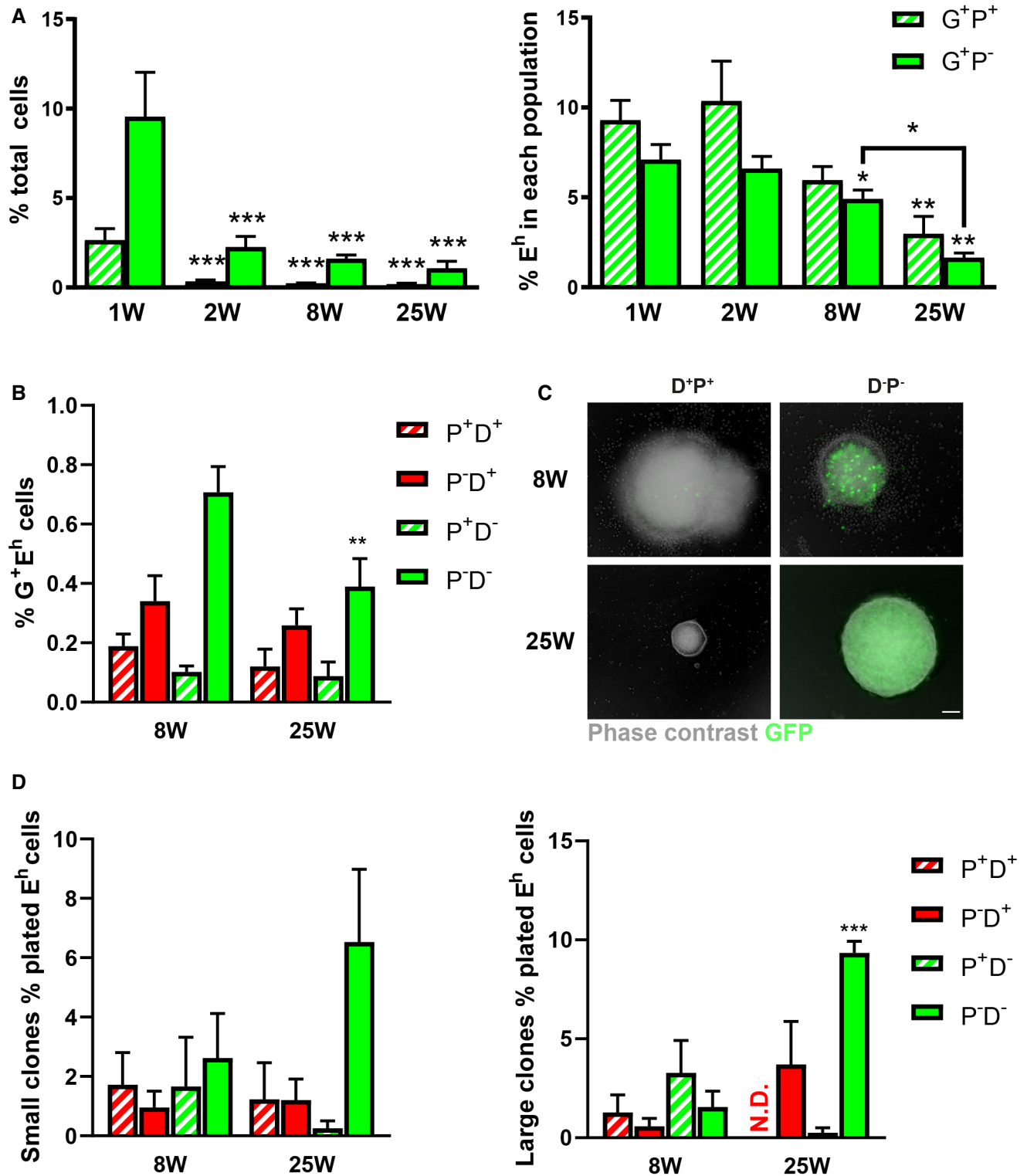


Figure 4.

Figure 4. Basal NSCs represent the predominant stem cell population in the adult V-SVZ.

- A Quantification of the flow cytometry analysis illustrating the number of apical Prominin-1-immunopositive (G^+P^+) and basal Prominin-1-immunonegative (G^+P^-) H2B-GFP-expressing cells (left panel) and of the percentage of activated cells expressing high levels of EGFR (E^h) in each population (right panel) at the various ages as indicated.
- B Quantitative analysis of the percentage of Dil-labelled apical (D^+) and unlabelled basal (D^-) G^+E^h cells expressing Prominin-1 (P^+) or not (P^-) in the V-SVZ of 8- and 25-W-old animals.
- C Representative micrographs of clonal neurospheres generated from G^+E^h cells isolated at the indicated ages and displaying H2B-GFP (GFP), Dil-labelling and Prominin-1 immunoreactivity. Scale bar = 100 μ m.
- D Quantification of the percentage of the indicated subsets of G^+E^h cells generating small (left panel) and large (right panel) clones after sorting from 8W or 25W animals.

Data information: Bars represent mean \pm SEM. N.D., none detected. $N \geq 6$ biological replicates. *Indicates in (A) a significant difference from the corresponding 1 W population (on top of bars) or between ages (lines), in (B) from the respective population at 8 W. * $P < 0.05$, ** $P < 0.01$, *** $P < 0.001$, determined by two-way ANOVA with Sidak's multiple comparisons test.

have previously shown that most OB adult-born neurons are derived from NSCs in the V-SVZ, which we tagged with a minimal GFAP promoter (Weber *et al*, 2011). However, since the promoter is active in both apical and basal cells, it is not clear whether both pools of NSCs contribute to neurogenesis. To address these points, we selectively tagged apical V-SVZ cells by intraventricular injection of recombinant adeno-associated viral (AAV) particles, driving the constitutive expression of GFP in adult WT mice (Luque-Molina *et al*, 2019). We first used this approach to investigate the lineage relationship between apical and basal NSCs. Analysis of coronal brain slices 14 days and 6 weeks after injection showed that at both timepoints the overwhelming majority of GFP^+ cells were represented by apical cells (Appendix Fig S5A). The rare basal GFP^+ cells 14 days after the injection were virtually all non-cycling (Appendix Fig S5B), showing that they were not rapidly proliferating progenitors. Even 6 weeks after injection, GFP^+ cells displaying NSC markers like SOX9 and/or GFAP were consistently observed at the apical but not the basal side of the V-SVZ (Fig 5A). At the apical side, $GFP^-/SOX9^+/GFAP^+$ double-positive and $GFP^+/SOX9^+/GFAP^+$ triple-positive cells represented 5.0 ± 0.7 and 6.9 ± 1.1 of the total apical cell population (see also Appendix Fig S5C and D), confirming that our approach targets a consistent proportion of apical NSCs. Instead, although $GFP^-/SOX9^+/GFAP^+$ represented 13.9 ± 1.4 of the total basal cells, triple-positive $GFP^+/SOX9^+/GFAP^+$ constituted only 0.7 ± 0.1 of the total basal cell population (see also below Appendix Fig S5D). Most apical GFP^+ cells also expressed SOX9, consistent with previous observations showing the expression of this transcription factor in most ependymal cells (Scott *et al*, 2010; Sun *et al*, 2017).

To investigate whether GFP^+ cells are involved in neurogenesis, we next quantified doublecortin (DCX) expression and GFP labelling in the OB of injected mice (Fig 5B and C). At both 14 days and 6 weeks after AAV-GFP injection, we could find three types of labelled cells in the OB: a minority of cells with neuronal morphology expressed GFP only or both DCX and GFP, whereas the vast majority of immature neurons were labelled only with DCX (Fig 5B and C). Independent of the time of analysis, both types of GFP^+ cells represented a very small percentage of total cells, especially in the core of the OB where newly generated neurons switch migration mode (Appendix Fig S5E). Instead, single- and double-labelled cells could be readily observed even 8 weeks in the core of the OB after injection of AAV-GFP into the dorsal corner of the V-SVZ (Appendix Fig S5F). To further investigate whether basal NSCs contribute to neurogenesis, we injected AAV-hGFAP-mycCRE viral particles into RiboTag mice (Sanz *et al*, 2009) to drive the expression of mycCRE under the control of a minimal hGFAP promoter. This removes a floxed stop codon, thereby inducing the expression of an HA-tagged ribosomal marker in hGFAP-expressing cells. To selectively tag basal NSCs, we injected mice with either 1×10^6 or 0.5×10^6 particles in the basal corner of the V-SVZ and sacrificed the two groups of animals after 5 days and 8 weeks respectively. Irrespective of time and number of injected viral particles, we found similarly low numbers of tagged cells in the V-SVZ (Appendix Fig S5G). Moreover, the majority of these tagged cells were localized at the dorsal/medial side of the lateral V-SVZ, with a position of the nuclei compatible with them being basal NSCs. Consistent with this, most of these cells exhibited both haemagglutinin (HA) tagging of the ribosomes and mycCRE staining, showing

Figure 5. Basal NSCs contribute to neurogenesis in the OB.

- A Representative micrographs of coronal sections of WT mice intraventricularly injected with AAV-GFP, and stained for GFAP and SOX9 14 days after injection. Scale bar indicates 30 μ m. Arrows indicate apical GFP^+ (white) and basal GFP^- (green) NSCs labelled by SOX9 and GFAP.
- B Representative micrographs of the OB of AAV-GFP-injected animals, at 14 days (14D) and 6 weeks (6 W) after virus injection. Scale bar indicates 20 μ m.
- C Quantification of GFP^+ and/or DCX^+ cells in the OB, as a percentage of total DAPI cells $N \geq 5$.
- D, E Representative confocal images of coronal slices of the core of the olfactory bulb (OB) obtained from RiboTag mice injected with AAV-hGFAP-mycCRE particles. In (D), mice were analysed 8 weeks after injection in the lateral corner of the V-SVZ. Arrow in point at Doublecortin (DCX)-immunopositive neuroblasts displaying haemagglutinin-tagged ribosome (RiboTag-HA). In (E), mice were analysed 16 weeks after injection in the lateral ventricle or in the lateral corner as indicated. Scale bars = 20 μ m.
- F Quantification of RiboTag-HA (HA) $^+$ and/or DCX^+ cells in the OB in $N \geq 2$.
- G Number of apical and basal E^h cells counted by flow cytometry and given as a percentage of total G^+ cells in Virgin (Virg) and littermate dams that had been lactating for 7 days (Lact). $N \geq 5$.

Data information: N number refers to biological replicates; for each biological replicate (except G), at least three technical replicates were performed. Bars represent mean \pm SEM. *Indicates significance: * $P < 0.05$, determined by two-way ANOVA with Sidak's multiple comparisons test.

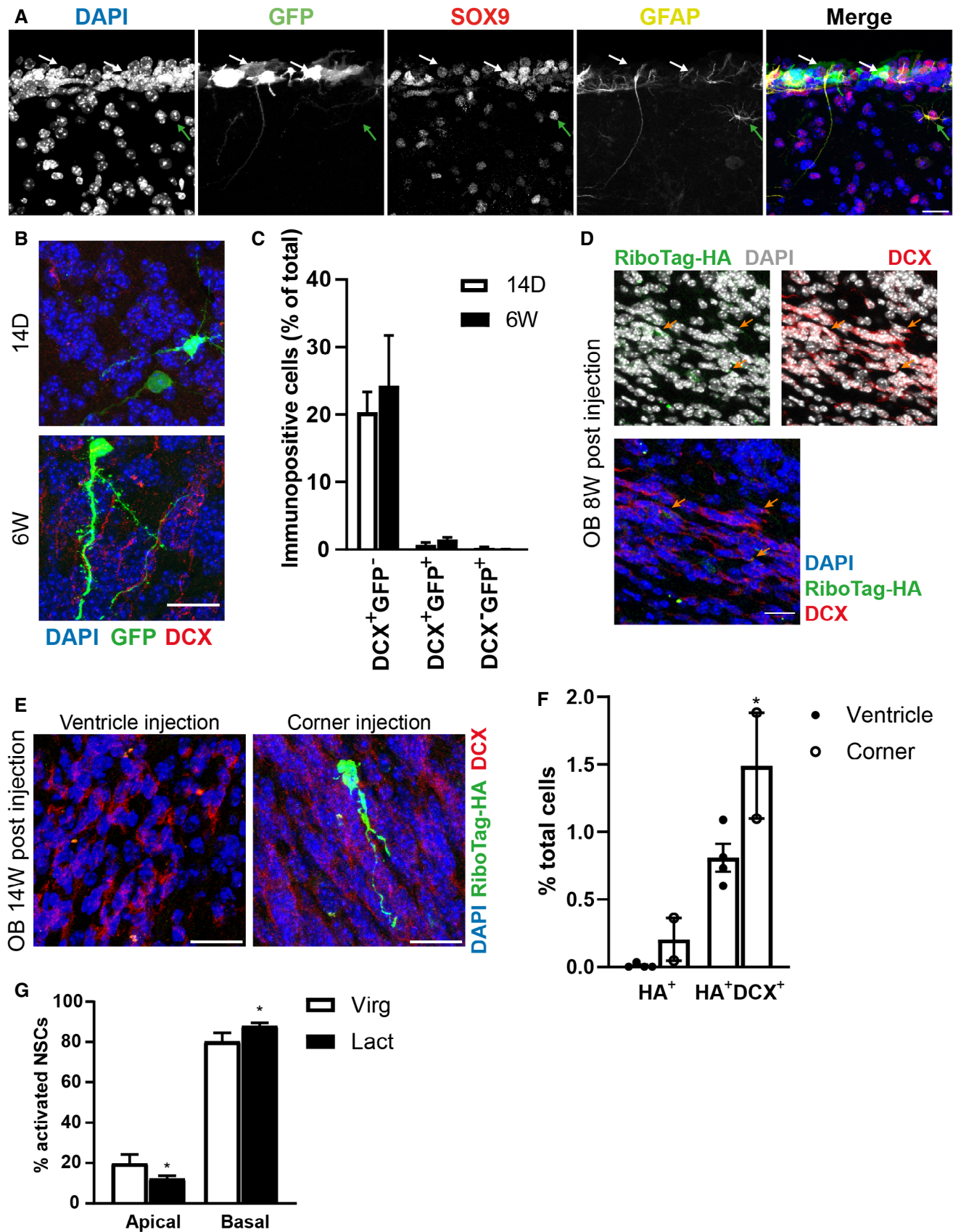


Figure 5.

recombination in progenitors still displaying hGFAP promoter activity (Appendix Fig S5G). Despite the very low number of cells tagged in the V-SVZ, we consistently observed RiboTag-HA-labelled neuroblasts in the core of the OB after 8 weeks (Fig 5D). Although we were able to permanently tag progenitors, we could not exclude the possibility that some hGFAP-tagged cells represent apical NSCs, as hGFAP is expressed in both apical and basal NSCs. Therefore, we next compared the effect of injecting AAV-hGFAP-mycCRE viral particles either in the dorsal corner of the V-SVZ or in the lateral ventricle and analysed the OB after 14 weeks (Fig 5E and F; Appendix Fig S5H). Even at this late time after injection, the OB of mice injected in the V-SVZ displayed a greater number of HA-labelled DCX⁺ young neurons than the OB of mice injected in the lateral ventricle (Fig 5E and F). Moreover, cells labelled with HA only and with mature neuronal morphology were readily observed in the OB of the first but of not the latter group of injected mice. Thus, although we could not take advantage of markers to selectively tag basal NSCs, both approaches of viral-mediated tagging of basal NSCs indicate that the latter are the main contributors to OB neurogenesis. However, in normal conditions, the generation of basal NSCs from apical NSCs may be difficult to detect due to the fact that slow-cycling apical NSCs rarely divide. Therefore, we next investigated the contribution of apical and basal NSCs to the physiological

increase in proliferation in the V-SVZ and OB neurogenesis that is elicited in female mice after 7 days of lactation (Shingo *et al*, 2003). For this analysis, we compared the proportion of apical and basal NSCs activated NSCs in the V-SVZ in control virgin female hGFAP; H2B-GFP mice and littermate dams, which had been lactating for 7 days (Fig 5G). Lactation led to a significant increase in the activation of basal and a parallel decrease cell cycle entry of apical NSCs (Fig 5G). This indicates that basal NSCs sustain the increased generation of neuronal progenitors and it supports our previous evidence that basal NSCs are the main contributors to adult neurogenesis in the OB.

Regulators of NSC activation and Notch signalling are differentially expressed in apical and basal NSCs

Upon our reanalysis of the data in Beckervordersandforth *et al* (2010), we could identify upregulation of the PEDF signalling pathway in activated Prominin⁻/GFP⁺ cells (Appendix Table S1 and Dataset EV1) and differential regulation of genes associated with the Notch signalling pathway between the latter and Prominin⁺/GFP⁺ cells (Fig 6A and Appendix Fig S6A). Previous studies have revealed that PEDF acts as a niche-derived growth factor promoting NSC self-renewal by upregulating the expression of Notch-signalling

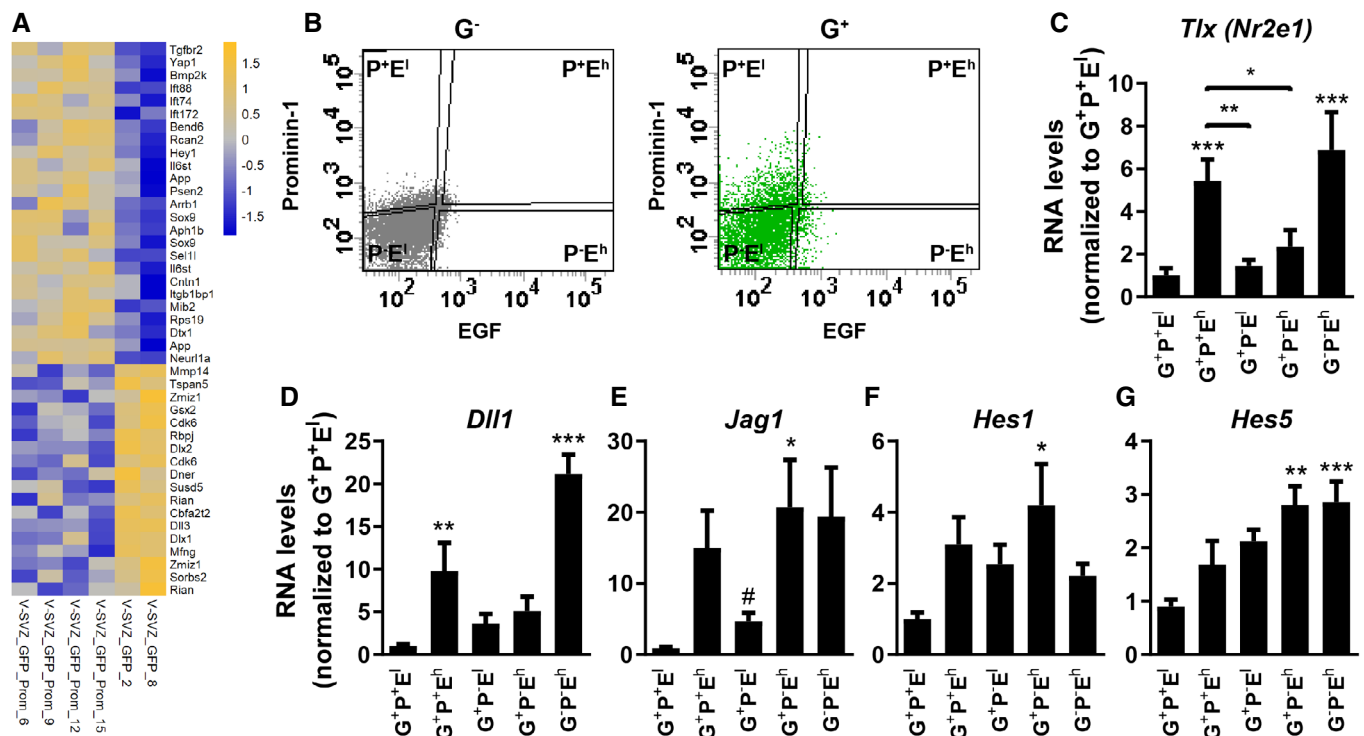


Figure 6. Expression of Notch signalling-related genes in NSCs of the V-SVZ.

A Heatmap illustrating differentially regulated Notch genes in hGFAP-eGFP (GFP) cells expressing Prominin-1 (Prom) as indicated.

B Representative FACS plots of G⁻ and G⁺ cells sorted for fluorescently labelled EGF and Prominin-1.

C–G Relative mRNA expression levels for the indicated genes.

Data information: Bars represent mean ± SEM, N ≥ 6 biological replicates; at least two technical replicates were performed. * and # indicate significance to G⁺P⁺E⁻ population or as indicated (lines), calculated by one-way ANOVA with Tukey's multiple comparisons test (*) or by Student's *t*-test (#). *[#]p < 0.05, ***p < 0.01, ****p < 0.001.

effector genes *Hes1* and *Hes5* (Ramirez-Castillejo *et al*, 2006). We have recently found that the TLX/NR2E1–Notch axis coordinates activation and proliferation between apical and basal progenitors in the V-SVZ-regulating Notch signalling across the V-SVZ (Luque-Molina *et al*, 2019). However, the underlying molecular basis and the involvement of NSCs in this regulation are still poorly understood. To investigate this issue, we used quantitative RT–PCR to compare the expression of *Tlx* and various Notch signalling-related gene transcripts in apical $G^+P^+E^l$ and basal $G^+P^-E^l$ quiescent NSCs, in apical $G^+P^+E^h$ and basal $G^+P^-E^h$ -activated NSCs, and in $G^-P^-E^h$ transit-amplifying progenitors (TAPs; Fig 6B–G). Consistent with previous studies (Obernier *et al*, 2011; Li *et al*, 2012), we found that the expression of *Tlx* was significantly greater in apical activated $G^+P^+E^h$ NSCs as well as in $G^-P^-E^h$ TAPs compared to other cell types. In contrast, quiescent $G^+P^-E^l$ and activated $G^+P^-E^h$ basal NSCs did not show a significant regulation of *Tlx* expression (Fig 6C), indicating that the elevated expression of the orphan nuclear receptor is associated prominently with the activation of apical but not basal NSCs. Analysis of the transcript levels of the Notch ligands, i.e. *Delta1* (*Dll1*; Fig 6D) and *Jagged 1* (*Jag1*; Fig 6E), and of the most prominent Notch effector genes in the V-SVZ, i.e. *Hes1* (Fig 6F) and *Hes5* (Fig 6G), also revealed different expression profiles between the various apical and basal cell populations. For all genes analysed, including both Notch ligands, the lowest levels of gene expression were observed in apical quiescent $G^+P^-E^l$ NSCs. Basal quiescent $G^+P^-E^l$ cells also displayed low levels of *Dll1* expression but higher expression of *Jag1* than the apical counterpart. Consistent with previous findings (Kawaguchi *et al*, 2013), in both apical and basal NSCs, the expression levels of Notch ligands were positively correlated with NSC activation (Fig 6D and E). However, while apical NSCs activation was accompanied by an increase in the expression of both Notch ligands, in activated basal NSCs only *Jag1* transcript levels were significantly increased. Additional differences between apical and basal progenitors were observed with respect to the expression of effector genes. The levels of *Hes1* transcripts were upregulated in a comparable manner across the four remaining cell populations, whereas *Hes5* expression was increased only in basal cells, including TAPs (Fig 6E and F). Taken together, these data show a distinct distribution of genes associated with Notch signalling in NSCs and progenitors along the apical/basal axis of the V-SVZ. They also show that at both sides of the niche, NSC activation leads to the acquisition of a transcriptional profile which is characteristic of Notch signal-sending NSCs, whereas quiescent NSCs, especially at the apical side, essentially display a signature of Notch signal-receiving NSCs. Supporting this last conclusion, we also found that Notch signalling activation was stronger in ciliated NSCs and ependymal, which are most apical (Appendix Fig S6B and C).

Since the *Tlx*–*Hes1* axis plays a role in the activation of apical NSCs, we next aimed to downregulate *Hes1* expression specifically in apical NSCs via intraventricularly injected AAV constructs, as described before (Luque-Molina *et al*, 2019), to determine the effect on Notch activation and proliferation dynamics in apical and basal NSCs. This approach, in addition to apical NSCs, also targets *Hes1*-expressing ependymal cells (Stratton *et al*, 2019). Thus, we first used meta-analysis of the RNA-sequencing data collected, made available by the lab of Sten Linnarsson at Karolinska Institute, Sweden (Zeisel *et al*, 2018), on mousebrain.org, to investigate *Hes1*-

expression in ependymal cells (Appendix Fig S7) and to validate our approach. We found that within the ependymal population, the expression of *Hes1* was limited to a group of cells half of which were characterized by the expression of Nestin and/or GFAP (Appendix Fig S7A and B). Moreover, among ependymal cells, *Hes1*-positive cells population expressed the highest levels of radial glia markers, such as solute carrier family 1 member 3 (*Slc1a3*) and fatty acid binding protein 7 (*Fabp7*; Appendix Fig S7C). Taken together, these data indicate that at the apical side of the niche, *Hes1* is expressed mostly in NSCs and less in mature ependymal cells. We therefore proceeded with intraventricular injections of AAVs that drive the constitutive expression of GFP and either a *Hes1*-specific short hairpin (AAV-*Hes1*-sh) or a scramble control (AAV-sc-sh) (Luque-Molina *et al*, 2019) to investigate the effect of apical loss of *Hes1* function (Fig 7).

Independent of the constructs employed, 14 days after intraventricular AAV injection, GFP was expressed mainly by cells lining the lateral ventricle (Fig 7A and B). We next measured fluorescence levels of the Notch intracellular domain (NICD; Fig 7C), to quantify activation of Notch signalling, and Ki67 expression (Fig 7D), in order to measure the number of cycling cells in infected (GFP^+) and non-infected (GFP^-) at the apical and basal side of the V-SVZ. This analysis showed that, compared to the scramble control, injection of AAV-*Hes1*-sh affected NICD immunoreactivity across all groups examined including basal cells, showing that Notch signalling connects progenitors between the apical and basal sides of the niche. Downregulation of Notch signalling was accompanied by an increase in the number of cycling cells ($Ki67^+$) across all the populations examined, although this effect was stronger in apical than in basal cells (Fig 7D). Moreover, the increase in proliferation, even at the apical side, was also observed in GFP^- non-transduced cells, further underscoring the importance of cell–cell interactions for the regulation of proliferation in the V-SVZ.

Analysis of DCX expression 14 days after AAV injection revealed no effect of *Hes1* knockdown on the number of neuroblasts (Appendix Fig S8A). However, AAV-*Hes1*-sh infection resulted in a significant increase in the number of GFP^+/DCX^+ neuroblasts in the apical V-SVZ 6 weeks after injection (Appendix Fig S8A). At this time, downregulation of *Hes1* expression also led to an increase in the number of GFP^+ neurons in the OB (Fig 7E). Strikingly, at both 14 days and 6 weeks after injection of either viral construct, the vast majority of DCX^+ neuroblasts were represented by GFP^- cells. Independent of GFP expression, downregulation of *Hes1* did not affect SOX9 and/or GFAP expression at the apical V-SVZ 6 weeks after injection (Appendix Fig S8B). Expression of these markers was also not affected in GFP^- basal cells (Appendix Fig S8C right panel), showing that downregulation of *Hes1* does not affect astrocyte and NSC generation. However, the number of basal $GFP^+/SOX9^+$ cells was significantly increased after *Hes1* knockdown (Appendix Fig S8C left panel), suggesting that decreasing Notch signalling may promote the generation of apical $GFAP^-/SOX9^+$ basal progenitors. Taken together, these data show that in the V-SVZ, Notch signalling connects apical and basal progenitors, thereby repressing differentiating cell division across the V-SVZ and promoting neurogenesis and basal relocation in apical NSCs. However, this type of manipulation did not allow us to observe the immediate consequences of downregulation of Notch signalling in apical and basal NSCs. Therefore, we next exposed the whole V-SVZ to the γ -secretase inhibitor

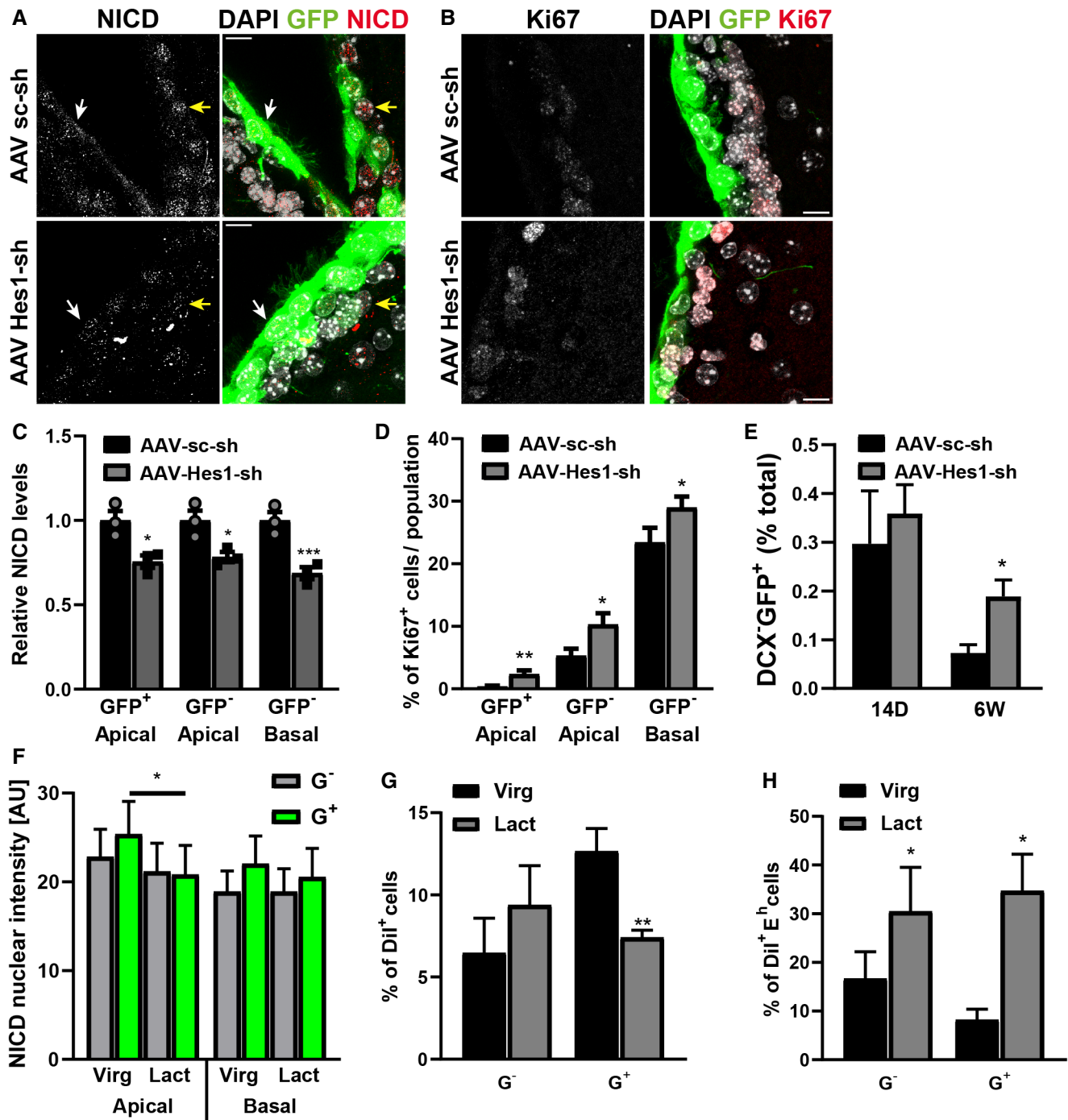


Figure 7. Interference with the Notch signaling pathway leads to increased proliferation.

A, B Representative micrographs of the V-SVZ of mice injected with an AAV overexpressing GFP and a shRNA against Hes1 (AAV Hes1-sh) or a scrambled sequence (AAV sc-sh). Coronal sections were stained with either Notch intracellular domain (NICD, A) or Ki67 to visualize cycling cells (B). DAPI was used for nuclear counterstain, scale bars indicate 20 μ m. Arrows indicate apical GFP⁺ (white) and basal GFP⁻ (yellow) cells displaying NICD staining.

C–E Quantification of fold change in NICD levels; $N = 3$ (C), Ki67⁺ cells; $N = 5$ (D) and GFP⁺DCX⁺ cells in the olfactory bulb (OB) 14 days (14D) and 6 weeks (6 W) after virus injection (E).

F–H Quantitative analysis illustrating NICD levels in apical and basal cells in virgin (Virg) and littermate dams that have been lactating for 7 days (Lact); $N = 11$ (F), the total percentage of apical G⁺ and G⁻ cells (G) and the percentage of activated cells in each population after 17 days of lactation. $N = 5$ (H).

Data information: N refers number of to biological replicates; for each biological replicate (except G + H), at least three technical replicates were performed. Bars represent mean \pm SEM. * $P < 0.05$, ** $P < 0.01$, *** $P < 0.001$, determined by two-way ANOVA with Sidak's multiple comparisons test (C–F) or two-tailed unpaired Student's t -test (G + H).

DAPT (N-[N-(3,5-difluorophenacetyl)-L-alanyl]-S-phenylglycine t-butyl ester) or the solvent dimethyl sulfoxide (DMSO) as a control, for 24 h before fixation and immunostaining with antibodies against Nestin and Ki67 (Appendix Fig S9). The treatment with DAPT resulted in an overall increase in the proportion of Ki67⁺ cells displaying high-intensity Ki67 staining (Appendix Fig S9A and C) and nuclear morphology of cells in meta- or anaphase, (Appendix Fig S9D). Blockade of Notch signalling also led to a significant increase in the percentage of G⁺Nestin⁺ and G⁺Ki67⁺Nestin⁺ triple-positive cells in the G⁺ population (Appendix Fig S9E and F). Notably, these effects were only significant at the apical and not at the basal side of the niche, supporting the view that inhibition of Notch signalling primarily affects apical NSCs.

We next investigated whether Notch signalling also changes during the physiological increase in basal NSC activation observed in lactating dams. Comparative analysis of NICD immunoreactivity between virgin female hGFAP;H2B-GFP mice and littermate lactating dams revealed a decrease in NICD immunoreactivity in the latter compared to the first (Fig 7F), consistent with our observations that lower Notch signalling leads to more proliferation in the V-SVZ. It is also consistent with previous findings showing that increased EGFR expression and proliferation in basal progenitors decrease Notch signalling in NSCs by a non-autonomous mechanism (Aguirre *et al.*, 2010). In this study, it also showed a parallel decrease in NSC self-renewal, as a consequence of lower Notch signalling. We therefore next investigated whether this regulation affects both apical and basal NSCs. For this, we determined the number of total apical and basal NSCs and the percentage of activated NSCs 14 and 17 days after lactation. The only significant change detected was a decrease in the number of apical NSCs after 17 days of lactation (Fig 7G). Moreover, at this time, the number of activated apical

NSCs was also increased, suggesting that apical NSCs undergo increased cell cycle entry to restore their cell number (Fig 7H). Taken together, although the full extent of Notch signalling involvement will require further investigation, our data indicate a scenario in which apical but not basal NSCs respond to increased progenitor proliferation in the V-SVZ by decreasing Notch signalling and proliferation.

Discussion

In this study, we show the presence of basal NSCs in the adult V-SVZ of the mouse brain for the first time. The diagram illustrated in Fig 8 summarizes the main phenotypic and functional differences observed between apical and basal NSCs. Notably, our data show that basal NSCs are responsible for the generation of most adult-born neurons arriving in the OB. Apical NSCs, in contrast, regulate the pace of differentiating cell division across the V-SVZ by instructing the strength of Notch activation across the niche, thereby acting as gate keepers for neurogenesis. It is well established that Notch signalling is essential to maintain stemness during quiescence of NSCs and ependymal cell differentiation (Carlen *et al.*, 2009; Imayoshi *et al.*, 2010; Kawaguchi *et al.*, 2013; Kawai *et al.*, 2017; Engler *et al.*, 2018; Than-Trong *et al.*, 2018). It is also known that interaction between Notch and EGFR signalling controls niche homeostasis by coordinating the proliferation of adult NSCs and more differentiated progenitors (Wang *et al.*, 2009; Aguirre *et al.*, 2010). However, the mechanisms underlying this regulation are still not clear as they were investigated in a situation of permanent upregulation of EGFR signalling. We show that these functions of Notch signalling are based on a directional distribution of Notch

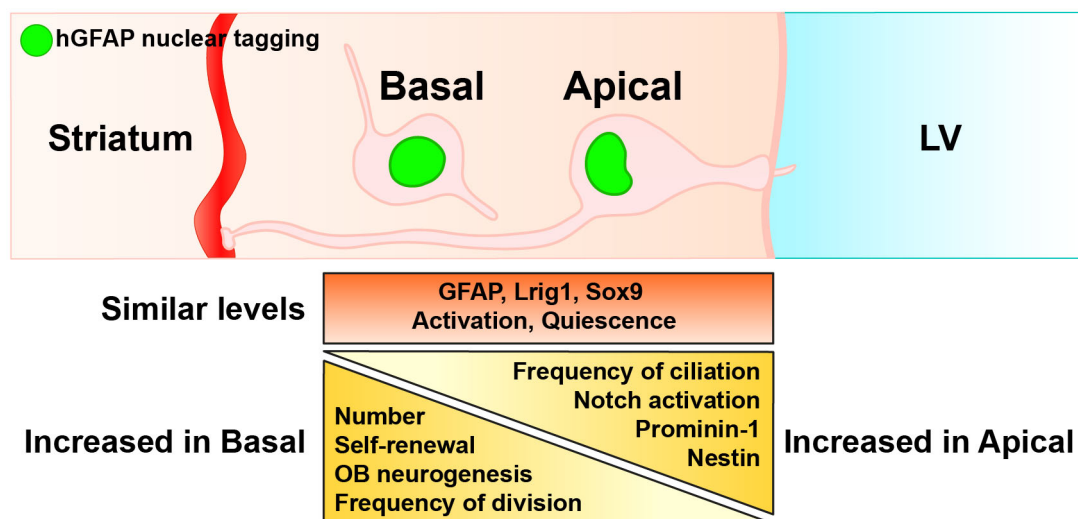


Figure 8. Schematic diagram summarizing main characteristics of apical and basal NSCs.

Both apical and basal NSCs are present in the adult V-SVZ. hGFAP promoter is active in both NSC groups. Apical and basal NSCs display similar levels of GFAP, Lrig1 and SOX9, but not of Nestin and Prominin-1 expression, which are prevalently observed in apical NSCs. Apical NSCs, like previously described radial glia-like/type B1 astrocytes, contact the lateral ventricle and often extend primary cilia. However, basal NSCs, similar to type B2 astrocytes in the V-SVZ, do not contact the lateral ventricle and rarely display primary cilia. Both NSC types undergo activation and quiescence and self-renewal *in vivo*. However, basal NSCs self-renew and proliferate more than apical NSCs *in vitro* and divide more frequently, and are the main contributors to OB neurogenesis than the apical counterpart *in vivo*. Apical and basal NSCs differ in the expression of genes associated with Notch signalling and the highest levels of activation are observed in apical NSCs.

ligands which increase not only according to lineage progression, as reported before (Kawaguchi *et al*, 2013), but also along the apical/basal axis of the V-SVZ, thereby providing apical NSCs with essential characteristics of Notch-receiving cells. Analysis of transcriptional signatures also indicates that different modulators of Notch signalling play a role in apical and basal NSCs. Whereas PEDF seems to regulate Notch signalling in basal NSCs, apical NSCs, possibly in light of their characteristics of Notch-receiving cells, are more responsive to the change in the number of progenitors. The crosstalk between EGFR and Notch signalling in the regulation of niche homeostasis was investigated before (Aguirre *et al*, 2010). We provide here evidence that similar crosstalk may occur in the context of a transitory increase in the number of proliferating progenitors the following lactation.

The identity of NSCs in the V-SVZ has been the object of numerous studies. Despite past disagreements on the nature of NSCs, according to the general consensus, radial glia-like apical cells are the main source of OB neurogenesis (Doetsch *et al*, 1999; Johansson *et al*, 1999; Beckervordersandforth *et al*, 2010; Codega *et al*, 2014; Nam & Capocchi, 2020). In contrast with this view, we here discovered the presence of basal NSCs in the adult V-SVZ. Previous work on transcriptional characterization of cells in the adult V-SVZ has also provided evidence for the presence of different pools of NSCs (Mich *et al*, 2014; Luo *et al*, 2015; Dulken *et al*, 2017; Morizur *et al*, 2018). Some of these previous work have also included the characterization of Prominin-immunopositive cells, which like the apical NSCs described here, displayed radial glia-like characteristics and included both activated and quiescent cells (Llorens-Bobadilla *et al*, 2015). It was also shown that these NSCs could give rise to new neurons in the OB upon isolation and transplantation in the V-SVZ, unlike the apical NSCs described here. This is consistent with our hypothesis that niche interactions and, in particular, Notch-mediated interactions regulate the ability of apical NSCs to contribute to neurogenesis. However, this work did not investigate the localization of the various NSC pools in the niche, pointing essentially at the correspondence of different NSC pools with different degrees of quiescence and activation to highlight stem cell heterogeneity. Previous analyses focusing on the position of neural progenitors in the V-SVZ have also underscored the complexity and the heterogeneity of niche progenitors. For example, it was recently shown that hGFAP-tagged apical progenitors include the majority ependymal-like and a minority with morphological characteristics of radial glia like NSCs (Joppe *et al*, 2020). Notably, hGFAP-tagged progenitors in this previous study displayed a slow division mode *in vivo* and *in vitro* and scarce and delayed contribution to neurogenesis. However, they were also shown incapable of undergoing activation and niche regeneration, raising the possibility that hGFAP is active in cells with morphological but not functional characteristics of NSCs. Whereas we have also observed that apical hGFAP scarcely contributes to neurogenesis, the apical NSCs studied here were still capable of undergoing activation and neurosphere generation, albeit to a lesser extent than the basal counterpart. A likely cause for the discrepancy between ours and the previous study is the different genetic models used. Unlike previous studies in which hGFAP was used to drive GFP expression, we here take advantage of hGFAP to induce the expression of a reporter whose levels are also controlled by cell division, which appears to result

in a more selective tagging of NSCs. Consistent with this, we found a direct relationship between levels of reporter expression and nuclear localization of tTA and very few neuroblasts within the tagged population. Notably, it was previously shown that the promoter is especially active in self-renewing, slow-cycling primary NSCs and that the activity of the promoter is downregulated in rapidly proliferating progeny, even if they maintain astroglial characteristics, which is consistent with the lack of more differentiated progeny in our hGFAP-tagged progenitors (Costa *et al*, 2011). Finally, our observation that tagged progenitors are neurogenic NSCs is in line with several published lineage tracing analyses. However, unlike the previous study, our data strongly indicate that basal and not apical hGFAP-tagged NSCs are the main contributors to OB neurogenesis.

Our study also provides a more unified view of the spatial organization of different pools of adult NSCs in the two main neurogenic niches. The presence of morphologically distinct types of NSCs, i.e. type 1 and type 2 (Steiner *et al*, 2006), has been long studied in the SGZ. Although both pools of hippocampal NSCs express radial glial markers in addition to SOX2 and SOX9 transcription factors (Suh *et al*, 2007; Sun *et al*, 2017), they are morphologically distinct, as only type 1 cells display a typical radial glia morphology with apical–basal polarity (Seri *et al*, 2001). In striking similarity with the differences between apical and basal NSCs in the V-SVZ reported here, it was observed that in the SGZ, type 1 radial NSCs consistently display Nestin and GFAP immunoreactivity although they are largely quiescent (Sun *et al*, 2017). In fact, in the adult SGZ, the expression of proliferation markers was mainly observed in non-radial NSCs, which like basal NSCs in the V-SVZ are the main contributors to steady-state neurogenesis and can actively proliferate in response to physiological stimuli (Lugert *et al*, 2010).

Although generally considered an NSC marker, Nestin immunoreactivity is not always observed in NSCs, especially if they are undergoing quiescence (Codega *et al*, 2014). Indeed, we here found that Nestin expression is significantly downregulated with increasing age and in quiescent apical NSCs. However, in adult basal NSCs, Nestin expression is virtually absent independent of the state of activation, suggesting that the expression of the intermediate filament is not only a function of the cell cycle state. Indeed, in the SGZ, Nestin is also expressed in radial NSCs, which are largely quiescent (Kempermann *et al*, 2004; Encinas *et al*, 2006). Notably, unlike in the V-SVZ, NSCs and progenitors in the SGZ all display primary cilia (Breunig *et al*, 2008; Amador-Arjona *et al*, 2011). Since we here found that the majority of ciliated apical NSCs extend primary cilia, it is possible that cilia-dependent signals promote Nestin expression. In the V-SVZ, primary cilia do not only regulate quiescence in radial glia and adult NSCs (Beckervordersandforth *et al*, 2010; Khatri *et al*, 2014) but they are also key to sensing signals present in the cerebrospinal fluid filling the ventricular cavity (Silva-Vargas *et al*, 2016; Monaco *et al*, 2019). Consistent with this view, recent observations have highlighted the possibility that in the V-SVZ, acquisition of quiescence occurs over a prolonged time period (Borrett *et al*, 2020) and involves different stages as well as the integration of multiple regulatory signals.

Thus, the postnatal V-SVZ contains two pools of NSCs that are exposed to different microenvironments and are differentially equipped to sense and transduce niche signals.

Material and Methods

Animals and V-SVZ dissection

All animal experiments were approved by the Regierungspräsidium Karlsruhe and the local authorities of Heidelberg University. The animal group size was calculated using G*Power3 and in compliance with the 3Rs guidelines. Mice were kept in a facility under a 12-h light/dark cycle and temperature- and humidity-controlled conditions, fed on a chow diet with *ad libitum* access to food and water. Males were mated to female mice aged between 8 and 16 weeks with a weight between 23 and 25 g. For FACS, C57BL/6 (Wildtype, WT) and hGFAP- τ TA;H2B-GFP (hGFAP;H2B-GFP) mice were sacrificed by CO₂ inhalation followed by cervical dislocation (adult), or by decapitation (neonatal). Doxycycline was administered for 4 weeks by adding it to the drinking water at a concentration of 50 mg/ml. A single intraperitoneal injection of IdU (Sigma-Aldrich; 100 mg/kg body weight) was administered to pregnant dams as indicated in the text. For DiI (1,1'-Dioctadecyl-3,3,3',3'-Tetramethylindocarbocyanine Perchlorate; Thermo Fisher Scientific) analyses, brains were placed on a Petri dish. After incision of the hemispheres, the exposed apical surface of the V-SVZ was labelled by applying DiI, dissolved in ethanol, for 1 min followed by washing in sort medium. Thereafter, the V-SVZ was dissected and further analysed as described below. To analyse the effect of lactation, hGFAP;H2B-GFP pregnant dams were sacrificed between 7 and 17 days after having given birth. Littermate virgin controls were sacrificed at the same time. For immunofluorescence WT, hGFAP;H2B-GFP and RiboTag mice (Sanz *et al*, 2009) were sacrificed by intracardial perfusion as described below.

Fluorescence-activated cell sorting

V-SVZ cells were dissociated and incubated at 4°C in a sort medium containing anti-Prominin1-APC, anti-Prominin-1-PE, or anti-Prominin-1-BV421 for 30 min. For experiments requiring EGFR labelling, cells were incubated for a further 30 min with recombinant human EGF conjugated to Alexa Fluor 488 or Alexa Fluor 647. Thereafter, cells were rinsed twice in a sort medium before being stained with propidium iodide (PI, 1:100) to stain dead cells and sorted with a FACSaria III flow cytometer (BD Biosciences, Heidelberg, Germany) as previously described (Ciccolini *et al*, 2005; Cesetti *et al*, 2009; Khatri *et al*, 2014). Unstained cells from the V-SVZ of WT and hGFAP;H2B-GFP mice were used to set gates for G⁻ and G⁺ cells and their respective autofluorescence levels. Dissociated V-SVZ cells from hGFAP;H2B-GFP mice stained with DiI, conjugated prominin antibodies, or fluorescently tagged EGF were used to set negative gates and compensations. For clonal analysis, FACS-sorted neural stem cells were plated for neurosphere formation as previously explained (Ciccolini *et al*, 2005).

For the analysis of self-renewal *in vivo*, we calculated the percentage of H2B-GFP-expressing (G⁺) cells displaying high or intermediate levels of fluorescence as described before (Luque-Molina *et al*, 2017). Briefly, H2B-GFP fluorescence levels were plotted on a logarithmic scale between the values of 10² and 10⁵. Based on negative controls, fluorescence levels around 10², 10³ and 10⁴–10⁵ were considered negative, intermediate and high respectively.

For a detailed list of antibodies, please see Appendix Table S2.

RNA expression analysis and qPCR

RNA was isolated with Arcturus® PicoPure™ RNA Isolation Kit (Thermo Fisher Scientific) according to the manufacturer's protocol including DNase digestion. Cells were directly sorted into 100 μ l lysis buffer, vortexed and stored at -80°C until RNA isolation. For reverse transcription, 9 μ l purified RNA was incubated with 1 μ l Oligo(dT)15 primers (Promega) at 80°C for 3 min. M-MLV buffer, M-MLV reverse transcriptase enzyme (200 U/ μ l, Promega), dNTPs (10 mM) and RNase-free water were added to RNA and Oligo(dT)15 mix to reach a final volume of 20 μ l. cDNA synthesis was performed at 42°C for 60 min followed by 10 min at 80°C. cDNA was then preserved at -20°C until qPCR. mRNA levels for the genes of interest were measured using a StepOnePlus Real-time PCR system and TaqMan gene expression assays (Applied Biosystems): *Ascl1/Mash1* (ID: Mm04207567_g1), β -actin (ID: Mm01205647_g1), *Tlx* (ID: Mm00455855_m1), *Hes1* (ID: Mm01342805_m), *Hes5* (ID: Mm00439311_g1), *Dll1* (ID: Mm01279269_m1), *Jag1* (ID: Mm01270195_gh) and *Lrig1* (ID: Mm00456116_m1). Cycle threshold (Ct) values were each normalized to the respective β -actin value (= Δ Ct). $\Delta\Delta$ Ct was calculated by subtracting the Δ Ct value of each population from the Δ Ct of the G⁺P⁺E⁻ population (normalizing population).

Intraventricular injections

WT mice were injected in the lateral ventricle with 1 μ l of adeno-associated virus (AAV) with a plasmid-encoding short hairpin RNA-targeting *Hes1* under the control of a U6 promoter (AAV-*Hes1*-sh), or a scramble control sequence (AAV-sc-sh). Characteristics of the plasmid and procedures of injection were described previously (Luque-Molina *et al*, 2019). RiboTag mice were injected in the lateral corner of the V-SVZ with 1×10^6 or 0.5×10^6 of AVV-hGFAP; myc-CRE viral particles to drive the expression of a myc-tagged constitutively active CRE recombinase under the control of a human GFAP promoter (Tang *et al*, 2015). Mice were sacrificed and processed for immunostaining 5 days and 8 weeks after injections as described below.

Immunofluorescence

Whole-mount dissection and immunostaining were performed as described previously (Mirzadeh *et al*, 2008; Monaco *et al*, 2019). For DAPT treatment, freshly dissected E18 whole mounts were incubated in a well of a 24-well-plate containing 1 ml EuroMed-N (Euroclone) with 1x B27 supplement (Invitrogen) and with either a solvent control (dimethyl sulfoxide, DMSO) or 20 μ M DAPT (N-[N-(3,5-Difluorophenacetyl)-L-alanyl]-S-phenylglycine t-butyl ester; Sigma-Aldrich, D5942) in DMSO, for 24 h at 37°C, 5% CO₂.

For coronal sections, mice sedated with pentobarbital (400 mg/kg) were perfused with ice-cold phosphate-buffered saline (PBS) followed by 4% paraformaldehyde (PFA) in PBS, after which the brains were removed and postfixed in 3% PFA / 4% sucrose in PBS for 48 h at 4°C. Brains were then cryoprotected by submersion in 30% sucrose in PBS at 4°C for 24 h and sliced into 20–30 μ m coronal sections using a Leica CM1950 cryostat (Leica Microsystems, Wetzlar, Germany). The sections were stored in PBS containing 0.01% sodium azide at 4°C until immunostaining. Slices were

permeabilized with 0.5% NP-40 in PBS for 5 min, then incubated in 10 mM glycine for 30 min for reduction of background fluorescence. Slices were blocked with 5% foetal calf serum (FCS) in PBS for 1 h, and incubated with primary antibodies in PBS at 4°C overnight. After washing, secondary antibodies were applied in 5% FCS in PBS containing 4',6-diamidino-2-phenylindole (DAPI) for nuclear counterstain for 2 h. Slices were then washed and mounted in Mowiol. All steps were performed at room temperature if not otherwise indicated. Slices and whole mounts that were to be directly compared in terms of protein expression and fluorescence level were stained in parallel using the same antibodies and dilutions. Immunofluorescence on sorted cells was performed as previously described (Khatri et al, 2014). A detailed list of primary antibodies used is provided in Appendix Table S3.

Imaging

Coronal sections and whole mounts were imaged using a Leica SP8 laser scanning confocal microscope. Images were acquired as z-stacks with 1 µm steps or 0.5–0.7 µm steps for cilia imaging. The imaging settings (laser intensity, gain and offset) were kept consistent for each experiment to ensure comparability.

Transcriptome analysis by microarray

Transcriptome analysis was performed on the RNA microarray dataset from Beckervordersandforth et al (2010), available on the Gene Expression Omnibus (GEO) database (<http://www.ncbi.nlm.nih.gov/gds>), accession number GSE18765. Briefly, ependymal and GFP-expressing cells, coexpressing Prominin-1 or not, were isolated by FACS from the V-SVZ and the diencephalon of hGFAP-eGFP mice. Expression was analysed after hybridization of total RNA from each cell group on Affymetrix MOE430 2.0 arrays. GFP⁺Prom⁺ and GFP⁺ samples were normalized with the Transcriptome Analysis Console (TAC; version 4.0.1.36; Thermo Fisher Scientific) using standard RMA settings. TAC was also used for the PCA of all samples. Statistical analysis was done as described in Beckervordersandforth et al (2010) and genes with a raw *P*-value < 0.05 were used to define the set of 4,713 regulated genes. Additional filters for fold-change > 1.3x and linear average expression > 100 in at least one group were applied. Heatmaps were generated in R. Pathway analyses were done through the use of QIAGEN's Ingenuity Pathway Analysis (IPA®, QIAGEN Redwood City, qiagen.com) using Fisher's exact test *P*-values. Genes involved in Notch signalling were obtained from Gene Ontology (GO:0007219).

Statistical analysis

Immunopositive cells were counted and normalized to the total number of cells (identified by DAPI-stained nuclei) or as stated otherwise. For quantification of cells in the V-SVZ, we defined cells as apical if their nuclei were located within the first two rows of nuclei bordering the lateral ventricle. Three regions of each slice were analysed in a 30,000 µm² -sized picture aligned with the longest axis of the apical side of the V-SVZ: dorsal, medial and ventral. Fiji/ImageJ software (Schindelin et al, 2012) was used for fluorescence intensity measurement and normalization to background levels.

During analysis, the pictures were labelled by treatment (i.e. doxycycline, DAPT, scramble/Hes1 shRNA and pregnancy) at all times and were not randomized or blinded.

Statistical significance was determined by two-tailed homoscedastic (or paired, when appropriate) Student's *t*-test for comparing two datasets, and one-way or two-way ANOVA with Tukey's or Sidak's multiple comparisons test for comparing more than two datasets. The analyses were performed using GraphPad Prism software. Significance was reached for **P* < 0.05, ***P* < 0.01 and ****P* < 0.001. Graphs represent mean values ± SEM.

Data availability

In this study, no primary datasets have been generated or deposited in external repositories.

Expanded View for this article is available online.

Acknowledgements

K.B. was supported by the Interdisciplinary Center for Neuroscience (IZN) and the Landesgraduiertenförderung (LGF) of the Heidelberg University Graduate Academy. The authors would like to thank Inma Luque-Molina for her help with clonal analysis. We would also like to thank the Department of Neurobiology for its continued support and the C-FACS facility for flow cytometry services. Open Access funding enabled and organized by Projekt DEAL.

Author contributions

Katja Baur: Data curation; formal analysis; investigation; visualization; writing – original draft; writing – review and editing. **Yomn Abdullah:** Formal analysis; investigation; writing – original draft. **Claudia Mandl:** Investigation. **Gabriele Hölzl-Wenig:** Investigation. **Yan Shi:** Investigation. **Udo Edelkraut:** Investigation. **Priti Khatri:** Investigation. **Anna M Hagenston:** Investigation; writing – review and editing. **Martin Irmeler:** Investigation; writing – review and editing. **Johannes Beckers:** Visualization. **Francesca Ciccolini:** Conceptualization; data curation; investigation; writing – original draft; project administration; writing – review and editing.

Disclosure and competing interests statement

The authors declare that they have no conflict of interest.

References

- Aguirre A, Rubio ME, Gallo V (2010) Notch and EGFR pathway interaction regulates neural stem cell number and self-renewal. *Nature* 467: 323–327
- Alves JA, Barone P, Engelender S, Froes MM, Menezes JR (2002) Initial stages of radial glia astrocytic transformation in the early postnatal anterior subventricular zone. *J Neurobiol* 52: 251–265
- Amador-Arjona A, Elliott J, Miller A, Ginbey A, Pazour GJ, Enikolopov G, Roberts AJ, Tersikh AV (2011) Primary cilia regulate proliferation of amplifying progenitors in adult hippocampus: Implications for learning and memory. *J Neurosci* 31: 9933–9944
- Anthony TE, Klein C, Fishell G, Heintz N (2004) Radial glia serve as neuronal progenitors in all regions of the central nervous system. *Neuron* 41: 881–890
- Beckervordersandforth R, Tripathi P, Ninkovic J, Bayam E, Lepier A, Stempfhuber B, Kirchhoff F, Hirrlinger J, Haslinger A, Lie DC et al (2010)

- In vivo* fate mapping and expression analysis reveals molecular hallmarks of prospectively isolated adult neural stem cells. *Cell Stem Cell* 7: 744–758
- Bishop GA, Barbari NF, Lewis J, Mykytyn K (2007) Type III adenylyl cyclase localizes to primary cilia throughout the adult mouse brain. *J Comp Neurol* 505: 562–571
- Borrett MJ, Innes BT, Jeong D, Tahmasian N, Storer MA, Bader GD, Kaplan DR, Miller FD (2020) Single-cell profiling shows murine forebrain neural stem cells reacquire a developmental state when activated for adult neurogenesis. *Cell Rep* 32: 108022
- Breunig JJ, Sarkisian MR, Arellano JJ, Morozov YM, Ayoub AE, Sojitra S, Wang B, Flavell RA, Rakic P, Town T (2008) Primary cilia regulate hippocampal neurogenesis by mediating sonic hedgehog signaling. *Proc Natl Acad Sci U S A* 105: 13127–13132
- Brill MS, Ninkovic J, Winpenny E, Hodge RD, Ozen I, Yang R, Lepier A, Gascon S, Erdelyi F, Szabo G et al (2009) Adult generation of glutamatergic olfactory bulb interneurons. *Nat Neurosci* 12: 1524–1533
- Carlen M, Meletis K, Goritz C, Darsalia V, Evergren E, Tanigaki K, Amendola M, Barnabe-Heider F, Yeung MS, Naldini L et al (2009) Forebrain ependymal cells are notch-dependent and generate neuroblasts and astrocytes after stroke. *Nat Neurosci* 12: 259–267
- Carrillo-Garcia C, Suh Y, Obernier K, Holzl-Wenig G, Mandl C, Ciccolini F (2010) Multipotent precursors in the anterior and hippocampal subventricular zone display similar transcription factor signatures but their proliferation and maintenance are differentially regulated. *Mol Cell Neurosci* 44: 318–329
- Cesetti T, Obernier K, Bengtson CP, Fila T, Mandl C, Holzl-Wenig G, Worner K, Eckstein V, Ciccolini F (2009) Analysis of stem cell lineage progression in the neonatal subventricular zone identifies EGFR+/NG2- cells as transit-amplifying precursors. *Stem Cells* 27: 1443–1454
- Ciccolini F, Mandl C, Holzl-Wenig G, Kehlenbach A, Hellwig A (2005) Prospective isolation of late development multipotent precursors whose migration is promoted by EGFR. *Dev Biol* 284: 112–125
- Codega P, Silva-Vargas V, Paul A, Maldonado-Soto AR, Deleo AM, Pastrana E, Doetsch F (2014) Prospective identification and purification of quiescent adult neural stem cells from their *in vivo* niche. *Neuron* 82: 545–559
- Costa MR, Ortega F, Brill MS, Beckervordersandforth R, Petrone C, Schroeder T, Gotz M, Berninger B (2011) Continuous live imaging of adult neural stem cell division and lineage progression *in vitro*. *Development* 138: 1057–1068
- Doetsch F, Garcia-Verdugo JM, Alvarez-Buylla A (1997) Cellular composition and three-dimensional organization of the subventricular germinal zone in the adult mammalian brain. *J Neurosci* 17: 5046–5061
- Doetsch F, Caille I, Lim DA, Garcia-Verdugo JM, Alvarez-Buylla A (1999) Subventricular zone astrocytes are neural stem cells in the adult mammalian brain. *Cell* 97: 703–716
- Dulken BW, Leeman DS, Boutet SC, Hebestreit K, Brunet A (2017) Single-cell transcriptomic analysis defines heterogeneity and transcriptional dynamics in the adult neural stem cell lineage. *Cell Rep* 18: 777–790
- Encinas JM, Vaahtokari A, Enikolopov G (2006) Fluoxetine targets early progenitor cells in the adult brain. *Proc Natl Acad Sci U S A* 103: 8233–8238
- Engler A, Rolando C, Giachino C, Saotome I, Erni A, Brien C, Zhang R, Zimmer-Strobl U, Radtke F, Artavanis-Tsakonas S et al (2018) Notch2 signaling maintains NSC quiescence in the murine ventricular-subventricular zone. *Cell Rep* 22: 992–1002
- Feierstein CE (2012) Linking adult olfactory neurogenesis to social behavior. *Front Neurosci* 6: 173
- Florio M, Huttner WB (2014) Neural progenitors, neurogenesis and the evolution of the neocortex. *Development* 141: 2182–2194
- Fuentealba LC, Rompani SB, Parraguez JI, Obernier K, Romero R, Cepko CL, Alvarez-Buylla A (2015) Embryonic origin of postnatal neural stem cells. *Cell* 161: 1644–1655
- Furuta M, Bridges RS (2005) Gestation-induced cell proliferation in the rat brain. *Brain Res Dev Brain Res* 156: 61–66
- Furutachi S, Miya H, Watanabe T, Kawai H, Yamasaki N, Harada Y, Imayoshi I, Nelson M, Nakayama KI, Hirabayashi Y et al (2015) Slowly dividing neural progenitors are an embryonic origin of adult neural stem cells. *Nat Neurosci* 18: 657–665
- Gage FH (2002) Neurogenesis in the adult brain. *J Neurosci* 22: 612–613
- Garcia AD, Doan NB, Imura T, Bush TG, Sofroniew MV (2004) GFAP-expressing progenitors are the principal source of constitutive neurogenesis in adult mouse forebrain. *Nat Neurosci* 7: 1233–1241
- Goto H, Inoko A, Inagaki M (2013) Cell cycle progression by the repression of primary cilia formation in proliferating cells. *Cell Mol Life Sci* 30: 3893–3905
- Harris L, Rigo P, Stiehl T, Gaber ZB, Austin SHL, Masdeu MDM, Edwards A, Urban N, Marciniak-Czochra A, Guillemot F (2021) Coordinated changes in cellular behavior ensure the lifelong maintenance of the hippocampal stem cell population. *Cell Stem Cell* 28: 863–876.e6
- Hockfield S, McKay RD (1985) Identification of major cell classes in the developing mammalian nervous system. *J Neurosci* 5: 3310–3328
- Hu XL, Chen G, Zhang S, Zheng J, Wu J, Bai QR, Wang Y, Li J, Wang H, Feng H et al (2017) Persistent expression of VCAM1 in radial glial cells is required for the embryonic origin of postnatal neural stem cells. *Neuron* 95: e306
- Imayoshi I, Sakamoto M, Yamaguchi M, Mori K, Kageyama R (2010) Essential roles of notch signaling in maintenance of neural stem cells in developing and adult brains. *J Neurosci* 30: 3489–3498
- Johansson CB, Momma S, Clarke DL, Risling M, Lendahl U, Frisen J (1999) Identification of a neural stem cell in the adult mammalian central nervous system. *Cell* 96: 25–34
- Joppe SE, Cochard LM, Levros LC Jr, Hamilton LK, Ameslon P, Aumont A, Barnabe-Heider F, Fernandes KJ (2020) Genetic targeting of neurogenic precursors in the adult forebrain ventricular epithelium. *Life Sci Alliance* 3: e202000743
- Kalman M, Pritz MB (2001) Glial fibrillary acidic protein-immunopositive structures in the brain of a crocodylian, *Caiman crocodylus*, and its bearing on the evolution of astroglia. *J Comp Neurol* 431: 460–480
- Kawaguchi D, Furutachi S, Kawai H, Hozumi K, Gotoh Y (2013) Dll1 maintains quiescence of adult neural stem cells and segregates asymmetrically during mitosis. *Nat Commun* 4: 1880
- Kawai H, Kawaguchi D, Kuebrich BD, Kitamoto T, Yamaguchi M, Gotoh Y, Furutachi S (2017) Area-specific regulation of quiescent neural stem cells by Notch3 in the adult mouse subependymal zone. *J Neurosci* 37: 11867–11880
- Kempermann G, Jessberger S, Steiner B, Kronenberg G (2004) Milestones of neuronal development in the adult hippocampus. *Trends Neurosci* 27: 447–452
- Khatri P, Obernier K, Simeonova IK, Hellwig A, Hölzl-Wenig G, Mandl C, Scholl C, Wolf S, Winkler J, Gaspar JA et al (2014) Proliferation and cilia dynamics in neural stem cells prospectively isolated from the SEZ. *Sci Rep* 4: 3803
- Kriegstein AR, Gotz M (2003) Radial glia diversity: a matter of cell fate. *Glia* 43: 37–43
- Li S, Sun G, Murai K, Ye P, Shi Y (2012) Characterization of TLX expression in neural stem cells and progenitor cells in adult brains. *PLoS One* 7: e43324
- Llorens-Bobadilla E, Zhao S, Baser A, Saiz-Castro G, Zwadlo K, Martin-Villalba A (2015) Single-cell transcriptomics reveals a population of dormant

- neural stem cells that become activated upon brain injury. *Cell Stem Cell* 17: 329–340
- Lois C, Garcia-Verdugo JM, Alvarez-Buylla A (1996) Chain migration of neuronal precursors. *Science* 271: 978–981
- Lugert S, Basak O, Knuckles P, Haussler U, Fabel K, Gotz M, Haas CA, Kempermann G, Taylor V, Giachino C (2010) Quiescent and active hippocampal neural stem cells with distinct morphologies respond selectively to physiological and pathological stimuli and aging. *Cell Stem Cell* 6: 445–456
- Luo J, Chen X, Pan YW, Lu S, Xia Z, Storm DR (2015) The type 3 adenylyl cyclase is required for the survival and maturation of newly generated granule cells in the olfactory bulb. *PLoS One* 10: e0122057
- Luque-Molina I, Khatri P, Schmidt-Edelkraut U, Simeonova IK, Holz-Wenig G, Mandl C, Ciccolini F (2017) Bone morphogenetic protein promotes Lewis X stage-specific embryonic antigen 1 expression thereby interfering with neural precursor and stem cell proliferation. *Stem Cells* 35: 2417–2429
- Luque-Molina I, Shi Y, Abdullah Y, Monaco S, Holz-Wenig G, Mandl C, Ciccolini F (2019) The orphan nuclear receptor TLX represses Hes1 expression, thereby affecting NOTCH signaling and lineage progression in the adult SEZ. *Stem Cell Reports* 13: 132–146
- Malatesta P, Hack MA, Hartfuss E, Kettenmann H, Klinkert W, Kirchhoff F, Gotz M (2003) Neuronal or glial progeny: regional differences in radial glia fate. *Neuron* 37: 751–764
- Merkle FT, Mirzadeh Z, Alvarez-Buylla A (2007) Mosaic organization of neural stem cells in the adult brain. *Science* 317: 381–384
- Mich JK, Signer RA, Nakada D, Pineda A, Burgess RJ, Vue TY, Johnson JE, Morrison SJ (2014) Prospective identification of functionally distinct stem cells and neurosphere-initiating cells in adult mouse forebrain. *Elife* 3: e02669
- Ming GL, Song H (2011) Adult neurogenesis in the mammalian brain: significant answers and significant questions. *Neuron* 70: 687–702
- Mirzadeh Z, Merkle FT, Soriano-Navarro M, Garcia-Verdugo JM, Alvarez-Buylla A (2008) Neural stem cells confer unique pinwheel architecture to the ventricular surface in neurogenic regions of the adult brain. *Cell Stem Cell* 3: 265–278
- Misson JP, Austin CP, Takahashi T, Cepko CL, Caviness VS Jr (1991) The alignment of migrating neural cells in relation to the murine neopallial radial glial fiber system. *Cereb Cortex* 1: 221–229
- Monaco S, Baur K, Hellwig A, Hölzl-Wenig G, Mandl C, Ciccolini F (2019) A flow cytometry-based approach for the isolation and characterization of neural stem cell primary cilia. *Front Cell Neurosci* 12
- Morizur L, Chicheportiche A, Gauthier LR, Daynac M, Boussin FD, Mouthon MA (2018) Distinct molecular signatures of quiescent and activated adult neural stem cells reveal specific interactions with their microenvironment. *Stem Cell Reports* 11: 565–577
- Nam HS, Capecchi MR (2020) Lrig1 expression prospectively identifies stem cells in the ventricular-subventricular zone that are neurogenic throughout adult life. *Neural Dev* 15: 3
- Obernier K, Alvarez-Buylla A (2019) Neural stem cells: Origin, heterogeneity and regulation in the adult mammalian brain. *Development* 146
- Obernier K, Simeonova I, Fila T, Mandl C, Holz-Wenig G, Monaghan-Nichols P, Ciccolini F (2011) Expression of Tlx in both stem cells and transit amplifying progenitors regulates stem cell activation and differentiation in the neonatal lateral subependymal zone. *Stem Cells* 29: 1415–1426
- Obernier K, Cebrian-Silla A, Thomson M, Parraguez JI, Anderson R, Guinto C, Rodas Rodriguez J, Garcia-Verdugo JM, Alvarez-Buylla A (2018) Adult neurogenesis is sustained by symmetric self-renewal and differentiation. *Cell Stem Cell* 22: 221–234.e8
- Ortiz-Alvarez G, Daclin M, Shihavuddin A, Lansade P, Fortoul A, Faucourt M, Clavreul S, Lalioti ME, Taraviras S, Hippenmeyer S et al (2019) Adult neural stem cells and multiciliated ependymal cells share a common lineage regulated by the geminin family members. *Neuron* 102: 159–172.e7
- Penisson M, Ladewig J, Belvindrah R, Francis F (2019) Genes and mechanisms involved in the generation and amplification of basal radial glial cells. *Front Cell Neurosci* 13: 381
- Ramirez-Castillejo C, Sanchez-Sanchez F, Andreu-Agullo C, Ferron SR, Aroca-Aguilar JD, Sanchez P, Mira H, Escribano J, Farinas I (2006) Pigment epithelium-derived factor is a niche signal for neural stem cell renewal. *Nat Neurosci* 9: 331–339
- Reynolds BA, Weiss S (1992) Generation of neurons and astrocytes from isolated cells of the adult mammalian central nervous system. *Science* 255: 1707–1710
- Sanz E, Yang L, Su T, Morris DR, McKnight GS, Amieux PS (2009) Cell-type-specific isolation of ribosome-associated mRNA from complex tissues. *Proc Natl Acad Sci U S A* 106: 13939–13944
- Schindelin J, Arganda-Carreras I, Frise E, Kaynig V, Longair M, Pietzsch T, Preibisch S, Rueden C, Saalfeld S, Schmid B et al (2012) Fiji: An open-source platform for biological-image analysis. *Nat Methods* 9: 676–682
- Scott CE, Wynn SL, Sesay A, Cruz C, Cheung M, Gomez Gaviro MV, Booth S, Gao B, Cheah KS, Lovell-Badge R et al (2010) SOX9 induces and maintains neural stem cells. *Nat Neurosci* 13: 1181–1189
- Seri B, Garcia-Verdugo JM, McEwen BS, Alvarez-Buylla A (2001) Astrocytes give rise to new neurons in the adult mammalian hippocampus. *J Neurosci* 21: 7153–7160
- Shen Q, Wang Y, Kokovay E, Lin G, Chuang SM, Goderie SK, Roysam B, Temple S (2008) Adult SVZ stem cells lie in a vascular niche: A quantitative analysis of niche cell-cell interactions. *Cell Stem Cell* 3: 289–300
- Shingo T, Gregg C, Enwere E, Fujikawa H, Hassam R, Geary C, Cross JC, Weiss S (2003) Pregnancy-stimulated neurogenesis in the adult female forebrain mediated by prolactin. *Science* 299: 117–120
- Silva-Vargas V, Maldonado-Soto AR, Mizrak D, Codega P, Doetsch F (2016) Age-dependent niche signals from the choroid plexus regulate adult neural stem cells. *Cell Stem Cell* 19: 643–652
- Steiner B, Klempin F, Wang L, Kott M, Kettenmann H, Kempermann G (2006) Type-2 cells as link between glial and neuronal lineage in adult hippocampal neurogenesis. *Glia* 54: 805–814
- Stratton JA, Shah P, Sinha S, Crowther E, Biernaskie J (2019) A tale of two cousins: Ependymal cells, quiescent neural stem cells and potential mechanisms driving their functional divergence. *FEBS J* 286: 3110–3116
- Suh H, Consiglio A, Ray J, Sawai T, D'Amour KA, Gage FH (2007) *In vivo* fate analysis reveals the multipotent and self-renewal capacities of Sox2+ neural stem cells in the adult hippocampus. *Cell Stem Cell* 1: 515–528
- Sun W, Cornwell A, Li J, Peng S, Osorio MJ, Aalling N, Wang S, Benraiss A, Lou N, Goldman SA et al (2017) SOX9 is an astrocyte-specific nuclear marker in the adult brain outside the neurogenic regions. *J Neurosci* 37: 4493–4507
- Tang W, Szokol K, Jensen V, Enger R, Trivedi C, Hvalby O, Helm PJ, Looger LL, Sprengel R, Nagelhus EA (2015) Stimulation-evoked Ca²⁺ signals in astrocytic processes at hippocampal CA3-CA1 synapses of adult mice are modulated by glutamate and ATP. *J Neurosci* 35: 3016–3021
- Tavazoie M, Van der Veken L, Silva-Vargas V, Louissaint M, Colonna L, Zaidi B, Garcia-Verdugo JM, Doetsch F (2008) A specialized vascular niche for adult neural stem cells. *Cell Stem Cell* 3: 279–288

- Than-Trong E, Ortica-Gatti S, Mella S, Nepal C, Alunni A, Bally-Cuif L (2018) Neural stem cell quiescence and stemness are molecularly distinct outputs of the Notch3 signalling cascade in the vertebrate adult brain. *Development* 145: dev161034
- Tramontin AD, Garcia-Verdugo JM, Lim DA, Alvarez-Buylla A (2003) Postnatal development of radial glia and the ventricular zone (VZ): a continuum of the neural stem cell compartment. *Cereb Cortex* 13: 580–587
- Waghmare SK, Bansal R, Lee J, Zhang YV, McDermitt DJ, Tumber T (2008) Quantitative proliferation dynamics and random chromosome segregation of hair follicle stem cells. *EMBO J* 27: 1309–1320
- Wang L, Chopp M, Zhang RL, Zhang L, Letourneau Y, Feng YF, Jiang A, Morris DC, Zhang ZG (2009) The notch pathway mediates expansion of a progenitor pool and neuronal differentiation in adult neural progenitor cells after stroke. *Neuroscience* 158: 1356–1363
- Weber T, Baier V, Pauly R, Sahay A, Baur M, Herrmann E, Ciccolini F, Hen R, Kronenberg G, Bartsch D (2011) Inducible gene expression in GFAP+ progenitor cells of the SGZ and the dorsal wall of the SVZ-A novel tool to manipulate and trace adult neurogenesis. *Glia* 59: 615–626
- Weigmann A, Corbeil D, Hellwig A, Huttner WB (1997) Prominin, a novel microvilli-specific polytopic membrane protein of the apical surface of epithelial cells, is targeted to plasmalemmal protrusions of non-epithelial cells. *Proc Natl Acad Sci U S A* 94: 12425–12430
- Yuzwa SA, Borrett MJ, Innes BT, Voronova A, Ketela T, Kaplan DR, Bader GD, Miller FD (2017) Developmental emergence of adult neural stem cells as revealed by single-cell transcriptional profiling. *Cell Rep* 21: 3970–3986
- Zeisel A, Hochgerner H, Lonnerberg P, Johnsson A, Memic F, van der Zwan J, Haring M, Braun E, Borm LE, La Manno G et al (2018) Molecular architecture of the mouse nervous system. *Cell* 174: 999–1014.e22



License: This is an open access article under the terms of the Creative Commons Attribution-NonCommercial-NoDerivs License, which permits use and distribution in any medium, provided the original work is properly cited, the use is non-commercial and no modifications or adaptations are made.